LBL-24731
Preprint

Center for Advanced Materials

CAM

RECEIVED
LAWRENCE
BERKELEY LABORATORY
MAY 10 1988
LIBRARY AND
DOCUMENTS SECTION

Submitted to Journal of
Applied Polymer Science

Microstructural and Bulk Characterization of Two Poly(siloxane-imide) Multiblock Copolymers

R.J. Spontak and M.C. Williams

January 1988

TWO-WEEK LOAN COPY

This is a Library Circulating Copy
which may be borrowed for two weeks.

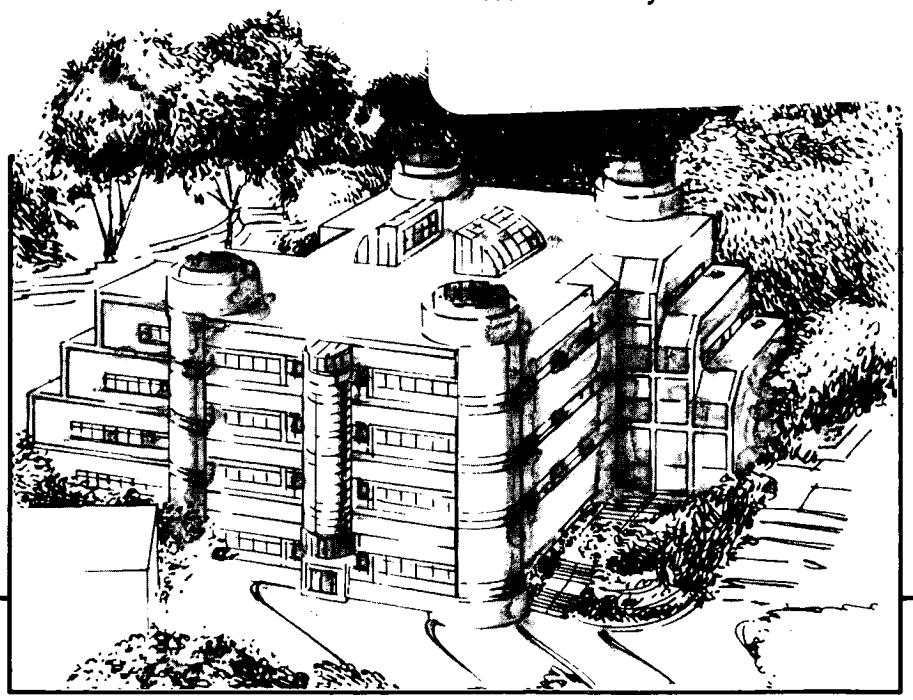

Materials and Chemical Sciences Division

Lawrence Berkeley Laboratory • University of California

ONE CYCLOTRON ROAD, BERKELEY, CA 94720 • (415) 486-4755

Prepared for the U.S. Department of Energy under Contract DE-AC03-76SF00098

LBL-24731

DISCLAIMER

This document was prepared as an account of work sponsored by the United States Government. While this document is believed to contain correct information, neither the United States Government nor any agency thereof, nor the Regents of the University of California, nor any of their employees, makes any warranty, express or implied, or assumes any legal responsibility for the accuracy, completeness, or usefulness of any information, apparatus, product, or process disclosed, or represents that its use would not infringe privately owned rights. Reference herein to any specific commercial product, process, or service by its trade name, trademark, manufacturer, or otherwise, does not necessarily constitute or imply its endorsement, recommendation, or favoring by the United States Government or any agency thereof, or the Regents of the University of California. The views and opinions of authors expressed herein do not necessarily state or reflect those of the United States Government or any agency thereof or the Regents of the University of California.

Microstructural and Bulk Characterization of Two Poly(siloxane-imide) Multiblock Copolymers

Richard J. Spontak and Michael C. Williams

Center for Advanced Materials
Lawrence Berkeley Laboratory
Berkeley, CA 94720-9989

and

Department of Chemical Engineering
University of California
Berkeley, CA 94720-9989

Correspondence should be addressed to:
Prof. Michael C. Williams
Dept. of Chemical Engineering
University of California
Berkeley, CA 94720-9989

SYNOPSIS

Much of the unique thermomechanical behavior of microphase-separated block copolymers is well established for the diblock and triblock architectures, and most of the data base involves polymers with polystyrene and polydiene blocks. However, there have been few reports about phase-separated multiblocks composed of polysiloxane blocks and polyimide blocks. Here, using various facets of electron microscopy, we have characterized the domain sizes and elemental composition of these copolymers. *In-situ* responses to both thermal annealing and tensile strain have been examined as well. To suggest possible structure-property relationships, differential scanning calorimetry and rheological tests have also been conducted. Measurements are reported for glass-transition and decomposition temperatures, linear viscoelastic properties (storage and loss moduli), and nonlinear stress-strain tensile properties.

INTRODUCTION

Block copolymers, composed of chemically dissimilar components, are known to undergo microphase separation due to thermodynamic incompatibility between the blocks under certain conditions of temperature, composition, molecular weight, and molecular architecture. The resultant microstructures, or domains, whose sizes are typically on the order of the polymer block end-to-end distances, are responsible for thermo-mechanical properties that are quite unlike those of either homopolymer or those of a random copolymer with identical composition. Microstructural parameters, such as the domain repeat distance, domain thickness, and the thickness of the interphase existing between the microphases, have been successfully quantified with the use of transmission electron microscopy (TEM)[1-5], small-angle X-ray scattering (SAXS)[6-9], and small-angle neutron scattering (SANS)[10-12]. Bulk mechanical and thermal properties, on the other hand, have been well-characterized by dynamic mechanical testing (DMT)[13-16] and differential scanning calorimetry (DSC)[17-20]. In general, the attempt to discern structure-property relationships in block copolymers has become a major focal point of many research efforts.

Most block copolymers are aimed at providing high-strength materials with bulk properties that allow for facilitated processing. One such copolymer is the poly(siloxane-imide) (*SiIm*) block copolymer. In this case, the imide polymer offers a wide variety of desirable characteristics. According to King and Lee[21] and Sweeting[22], polyimides are resistant to irradiation, mechanical deformation, and environmental and solvent attack, while still retaining exceptional thermooxidative and mechanical stability at elevated temperatures. Electrical properties, such as the dielectric constant and volume resistivity, are also insignificantly affected by temperature, thereby making this class of polymer ideally suited for a variety of applications including encapsulant and insulator.[23-26]

As Babu[27] points out, though, polyimides are generally intractable. This problem can be overcome by incorporating a flexible linkage into the polyimide. One successful attempt at doing

so is the polyetherimide, which becomes melt processable[28,29] because of the backbone ether link. Another method by which polyimides are made more tractable is the copolymerization with a rubbery polymer such as a polysiloxane. Silicone rubber, polydimethylsiloxane (PDMS), exhibits temperature stability, oxidative resistance, and physiological inertness, in addition to good electrical properties, but has a tensile strength of only 0.35 MPa. However, a block copolymer composed of both PDMS and imide blocks has been reported to possess a tensile strength of about 50 MPa.[30,31]

In this work, the microstructures of two different *SiIm* block copolymers are studied by utilizing various techniques of electron microscopy. Thermal and mechanical properties of *SiIm* cast films are investigated using DSC and DMT.

EXPERIMENTAL

Materials

Two *SiIm* block copolymers are used in this study. The first, produced by M&T Chemicals Inc. (Rahway, NJ 07065) through a polycondensation reaction,[32,33] is the 3510 grade multiblock (designated MT3 for brevity) and is characterized[34-36] in Table I. The general chemical structure[32-36] of this copolymer (Fig. 1) is described as a polyimide resin with siloxane blocks of the form $(\text{-Si-(R)}_2\text{-O-})_x$ incorporated directly into the polyimide backbone, with the soft segment comprised of this siloxane unit *and* a diamine linkage and the hard segment being the imide anhydride. The substituent groups of both the siloxane-diamine and anhydride blocks have not been revealed by the manufacturer, though we offer some speculation below. The sample was received in a 25% solution of N-methyl-2-pyrrolidone (NMP); dilute solutions were prepared with dry NMP and were used to cast films (see below) in a dry nitrogen atmosphere. NMP evaporation was conducted according to a cure cycle suggested by the manufacturer (1 hour at 100° C, 1 hour at 150° C, and 1 hour at 200° C), except where noted.

The second copolymer (GE1), a prototype produced by General Electric Co. (Pittsfield, MA 01201), is a multiblock copolymer with varying numbers (10-15) of siloxane segments in a block. Characterization data[37] are presented in Table I. The parent polyimide is the ULTEM-1000 polyetherimide, the structure[29] for which is presented in Fig. 2. Chloroform was used to dissolve the copolymer at room temperature[29,37]. Chloroform solutions were prepared to cast thin films, with solvent evaporation performed under the same conditions as above, although no "curing" was specified by the supplier.

Electron Microscopy

For conventional (low-voltage) transmission electron microscopy and analytical electron microscopy, ultrathin films or sections less than 100 nm thick are required. In this work, ultrathin films approximately 35 nm thick[3] were prepared by using a direct-casting technique (presented elsewhere[38]) from 0.5% solutions of both the MT3 and GE1 copolymers. [For slightly thicker GE1 films, 1.0% and 2.0% solutions were needed.] Since sufficient electron-absorption contrast exists between the imide and siloxane phases, staining was unnecessary. Static and stereo bright-field micrographs were obtained using a JEOL JEM 100CX electron microscope (JEOL Ltd., Peabody, MA 01960) at various magnifications with an accelerating voltage of 80 kV. Micrographs showing the *in-situ* curing nature of the MT3 copolymer were also acquired from this microscope with a heating stage attachment.

Direct observation of *in-situ* deformation of *SiIm* microstructures in each copolymer was accomplished by utilizing the capabilities[39] of the KRATOS 1.5 MeV electron microscope at the National Center for Electron Microscopy (Lawrence Berkeley Laboratory). Copolymer films were cast onto the 100-vertical (or horizontal)-mesh copper grid attachment of a strain stage, depicted in Fig. 3. Since Formvar was not used to provide support for the cast film, thicker sample films were required to be self-supportive; such films could still be examined using the greater accelerating vol-

tage of the KRATOS microscope. Once films measuring approximately 200-250 nm thick were cast from 2.0% solutions onto the grid attachment, the stage, which was designed to be completely reusable, was fitted into the straining attachment of the microscope. The sliding tracks and grid attachment are held in place by M-Bond 600 (Measurements Group, Raleigh, NC 27611), a solvent-thinned epoxy-phenolic adhesive. Tensile deformation at ambient temperature was performed at an elongation rate of 0.11-0.12 μm/sec, for periods of time up to 25 minutes.

Elemental analysis of the GE1 copolymer was accomplished using energy dispersive X-ray microanalysis on a JEOL JEM 200CX analytical electron microscope, operated at an accelerating voltage of 200 kV and equipped to use either a Kevex (Foster City, CA 94404) high-angle detector (HAD) or a Kevex ultrathin-window detector (UTW). The former, having a beryllium window, is able to detect only elements with atomic masses greater than sodium. The latter, with a parylene/aluminum window, is capable of detecting elements as light as carbon. To obtain a representative collection of light-element X-rays (e.g., carbon, oxygen, and nitrogen), samples were cooled in the microscope to -168° C with liquid nitrogen. Due once again to the lower voltage, ultrathin films were required.

Bulk Analyses

Thick films needed for DSC were prepared in much the same way as the ultrathin films. Here, concentrated solutions (25% for MT3 and 8% for GE1) were repeatedly cast until the desired thickness (≈ 0.5 mm) was attained. A Mettler FP84 differential scanning calorimeter (Mettler Instrument Corp., Highstown, NJ 08520), set on scan rates of 5°/min and 10°/min, was utilized to discern the thermal behavior of blocks cut from these films.

Both stress-strain and DMT were performed on the MT3 copolymer. An MTS Hydraulic Testing Apparatus (Minneapolis, MN 55424) was used to determine the stress-strain relationships of both the fully cured and partially cured copolymers: the former was cured according to the

suggested cure cycle, and the latter was cured for 2 hours at 85° C and 2 hours at 120° C. [The latter temperature was selected to be below the visibly detected yield temperature† of 130° C.] In both cases, the samples were cast from the as-received concentrated 25% solution onto Teflon to avoid adhesion difficulties. The resulting thick films, trimmed to resemble flat, rectangular sheets, measured approximately 0.5 mm in thickness for each sample studied. Sample thicknesses were measured with a micrometer. DMT was conducted with similar samples, using a Rheometrics Mechanical Spectrometer RMS-705 (Piscataway, NJ 08854). Measurements were made at temperatures up to 300° C in a dry nitrogen atmosphere using parallel plates, 25 mm in diameter and separated by 0.8 mm.

RESULTS AND DISCUSSION

Microstructural Characterization

Most previous studies of block copolymers have employed diblock and triblock molecules with nominally monodisperse molecular weights. We cannot expect *a priori* the same type of microstructure and properties from polydisperse multiblock copolymers which also are complicated by possessing composition distributions. For instance, Fig. 4 shows the fully developed microstructure in the MT3 copolymer after being fully cured. The dispersed domains are identifiable as being Si-rich because of their darkness. This rather small volume fraction of pure siloxane is not inconsistent with the soft segment constituting 74 wt% of the entire copolymer; these two facts together reveal that the siloxane is a minority component within the soft segment but has sufficiently long chains to segregate and form their own miniphase domains. (Larger domains involving the entire soft segment may exist, but the micrograph cannot reveal it.) A roughly bimodal size distribution of spherical domains is present, with the domain diameters averaging approximately 2-5 nm and 16

† Weights ranging from 10 to 50 g were suspended from films at ambient temperature. Upon heating, the films began to flow at 130° C, designated as the yield temperature.

nm in diameter. No hierarchical ordering of the domains is readily noticeable. Collectively, these features of domains are indicative of thermomechanical properties different from those exhibited by monodisperse diblock/triblock copolymers, which possess domain uniformity and well-established ordering.

Unlike the MT3 copolymer, the GE1 copolymer, when cast into ultrathin films, exhibited structure that was visible with an optical microscope. Nomarski differential contrast microscopy,[40] with reflected light at a magnification of 220×, was used to acquire the micrographs presented in Fig. 5. Microstructures appear to vary as the concentrations of solutions used to cast the films in Fig. 5 were increased from 0.5% (a) to 1.0% (b) to 2.0% (c). One noticeable difference between Fig. 5a and Figs. 5b and 5c is that most of the domains in Fig. 5a seem to have combined or stretched into elongated structures. Additional detail is provided by a series of TEM micrographs (Fig. 6) on similar samples. Again, there is a systematic change of microstructures as the casting-solution concentration increases -- i.e., as film thickness increases. The thinnest film (Fig. 6a) shows co-continuous elongated major phases (with an encapsulated miniphase) which gradually changes to large dispersed spherical (or cylindrical) phases (Fig. 6c) having thin interconnecting webs or ripples in the film. There is a corresponding change from a lateral orientation to isotropy. Such behavior is highly suggestive of dimensional constraints being imposed on the phase separation process. That is, a microphase whose (bulk) equilibrium configuration contains domains as large as seen in Fig. 6c will not be able to form such structures in films thinner than they (the structures) are. It is widely recognized, as well, that there are unique surface-energy effects in a film which is thinner than its equilibrium critical thickness,[41] the minimum sample thickness in which equilibrium structures can exist and retain properties of the bulk material.

The sizes of the domains in the GE1 copolymer vary from about tens of nanometers to several microns, which is quite unlike behavior observed in most block copolymers. One plausible explanation for this difference is that the copolymer was designed to have a specified *average* bulk

composition; consequently, the copolymer is composed of polymer molecules having a distribution of compositions (see Table I). Chains with a higher content of the dispersed-phase block would tend to swell the domains much in the same way as a homopolymer would. Another possibility is that simultaneous *macrophase* and *microphase* separation has occurred, in which the former is responsible for large domains and the latter for the small ones.

The size distribution of the resultant domains in the films cast from all three solutions is presented here in several ways. First, the distribution of projected dispersed-phase areas A_d was determined using an electronic graphics calculator manufactured by the Numonics Corp. (Lansdale, PA 19446). This area distribution, which accounts for all discrete albeit irregularly-shaped dark domains, is used to determine the domain equivalent diameters from $d_{eq} = (4A_d/\pi)^{1/2}$. Averages of both A_d and d_{eq} are tabulated in Table II. Despite varying film thickness and obvious morphological differences, the domains have an average $\bar{d}_{eq}$ of approximately 0.30 μm in all cases. The median d_{eq} is about 0.18 μm in all cases. Upon comparing $\bar{d}_{eq}$ with the average diameter ($\bar{d}$) of domains appearing two-dimensionally circular, we see that $\bar{d}$ approaches $\bar{d}_{eq}$ at higher solution concentrations and, hence, thicker films. This indicates that the domains in the thinnest films (Figs. 5a and 6a) are deformed due to internal stresses based upon the thickness of the film.

In addition to the size distribution of these dispersed domains, a distribution of domain aspect ratios -- the ratio of length to width of well-formed domains (i.e., those appearing as two-dimensional circles and ellipses in micrographs obtained from films varying in thickness) -- indicates that more than 70% of these domains have an aspect ratio of between 1.0 and 1.5 upon initial film casting. This information signifies that (a) some internal stresses were produced in the film as the solvent was evaporated but (b) these stresses were not sufficient enough to deform significantly the majority of the domains, especially in the thicker films prepared from the 1.0% and 2.0% solutions (where more "well-formed" domains were present).

Since the siloxane block comprises the minor component of this copolymer (≈ 40 wt%), the domains were initially expected to be silicone-rich. This is what one would also infer from the contrast exhibited between phases; that is, the siloxane block would normally appear darker due to an increase in the atomic number. However, an elemental analysis of this copolymer using energy-dispersive X-ray microanalysis[42,43] (EDX) on an analytical electron microscope revealed that the matrix, not the dispersed phase, was rich in silicon.

Examples of X-ray spectra for this copolymer are presented in Fig. 7. The domain, shown in Fig. 7a, exhibits a higher concentration of carbon than oxygen and silicon, which are about equally present. Chlorine, an artifact from the chloroform solvent, is also present in an appreciable quantity (> 1.0 wt%). In the matrix region (Fig. 7b), however, silicon is the most prevalent, followed by oxygen and then by carbon. No chlorine (meaning less than 1.0 wt%) was detected. [*Note:* Minor, unlabeled peaks in the spectra of Fig. 7 represent copper and aluminum, the former due to the TEM grids and the latter due to the sample holder.] Initial qualitative examination of these spectra indicate that the matrix is siloxane-rich and the domains represent imide-rich regions. An X-ray map of the copolymer is presented in Fig. 8 to substantiate this observation. In the lower right corner, a computer-generated image depicts the locations of the domains and matrix. The light areas in the remaining portions of the map illustrate the presence of silicon (upper left), carbon (lower left), and chlorine (upper right). Clearly, silicon is found in greater abundance in the matrix regions, and carbon and chlorine are more prevalent in the domains.

The only way that silicon-lean domains can appear darker than a silicon-rich matrix in transmission (lower right of Fig. 8) is for the domains to be thicker than the surrounding matrix, as shown schematically in Fig. 9. Further evidence of this topographical feature is seen upon closer examination of both the digitized image and silicon map, in which we see a "halo" region surrounding the domains which appears almost as an interphase and which shows a higher silicon content. A stereo view of this copolymer (Fig. 10) reveals definitive differences in topography.

Domains do, indeed, extend out of the film; and folds, or ripples, are also present. Consequently, we are forced to conclude that (a) the matrix, being siloxane-rich, constitutes the rubbery phase and (b) the domains are imide-rich and provide the stiffness required in this copolymer. The fact that the 40 wt%-phase is continuous is explained in part by its larger *volume* percentage (PDMS is less dense than the imide) and partly by its lesser thickness in the film (Fig. 9). A minority component can, of course, be a continuous phase up to a certain geometrical limit, and this may indeed be thermodynamically favored in some cases. Phase inversion such as this has been reported in ether-amide[44] and styrene-butadiene[45,46] block copolymers.

Quantitative information concerning the composition of the copolymer is acquired from the X-ray intensity counts by relating them to known samples through

$$\frac{C_A}{C_B} = k\frac{I_A}{I_B} \tag{1}$$

where C is the concentration, I is the intensity, A and B represent this sample and a reference sample, and k is the empirical "k-factor," values for which, given in Table III, can be obtained by experimental and theoretical means.[43] However, to account for the effects of absorption on the generated characteristic X-rays, k is modified according to

$$k^* = k\, f\,(P_z, \rho, t, \alpha_o) \tag{2}$$

where f is a well-characterized function[43] of P_z, the absorption coefficient; ρ, the material density; t, the sample thickness; and α_o, the X-ray incident angle. According to the manufacturer,[37] the average density of the siloxane block is estimated to be approximately 1.01-1.05 g/cm^3 and that of the imide block to be about 1.15-1.20 g/cm^3. [These values are in agreement with the average copolymer density, 1.10±0.10 g/cm^3, of the MT3 sample.[35]] Sample thicknesses are estimated to be about 80 nm.

Compositions, with and without absorption correction, are tabulated in Table IV for both the domain and matrix regions. Since absorption has little effect on this amorphous copolymer, the

conclusions reached above concerning phase distribution can now be fully quantified. From the domain to the matrix, the carbon content decreases from about 64 wt% to 46 wt%, whereas the silicon content roughly doubles. Oxygen seems to increase slightly, and the chlorine disappears completely. Further examination of these trends can be accomplished in much the same fashion in an X-ray trace (Fig. 11) across a domain. The compositions of carbon and chlorine increase from about 45 and 0 wt%, respectively, to about 70 and 1 wt%, respectively, from the matrix to domain and back to the matrix once again. The silicon, however, decreases from about 35 wt% to about 18 wt%. A slight maximum is again observed in the silicon composition between the central portions of the matrix and domain regions.

The fact that silicon is present in *both* phases presents a curious dilemma, which we now attempt to explain. One possibility for this observed phenomenon is that incomplete phase separation has occurred, as reported for some polyurethane block copolymers.[17,18,47] For instance, by comparing chemical nature differences (given as a Flory χ parameter or a solubility parameter difference) and ΔC_p measurements, Camberlin and Pascault[17,18] have determined the degree of phase segregation in several polyurethane systems. We can represent the degree of phase separation (Δ_S) in terms of the silicon concentration (C_{Si}) in the matrix:

$$\Delta_S \approx \frac{C_{Si}^{mat}}{C_{Si}^{mat} + C_{Si}^{dom}} \tag{3}$$

Here, C_{Si} is expressed in either wt% or atomic%, and *dom* and *mat* refer to the domain and matrix regions, respectively. Subsequently, Eq. 3 yields about Δ_S=0.67 phase separation using wt% compositions and 0.70 using atomic% compositions. This information is useful in predicting macroscopic properties, since such properties are direct functions of phase distribution (which is, in turn, a function of thermodynamics and local-scale kinetics).

One explanation for incomplete phase-separation behavior in this copolymer is due to the volatile nature of the chloroform solvent. Rapid solvent removal from the ultrathin films increases

the probability that blocks will be kinetically trapped in non-equilibrium configurations. This possibility, coupled with the fact that the copolymer is composed of a composition distribution (expressed as the block ratio in Table I), suggests that kinetic limitations are responsible for the presence of *Si* in both phases. Furthermore, the molecular composition distribution may account for the observed broad distribution of domain sizes. The block ratio, defined as the number of soft-segment blocks per imide block, is estimated to be about 10-15. Since the domains are, in many cases, significantly larger than the end-to-end distance of an imide block, domain swelling may be a dominant factor. For example, consider a part of a copolymer molecule in which a rather short *Si* block is situated between two lengthy Im blocks. Upon phase separation, the *Si* block may not be mobile enough to leave the Im domain and enter the *Si* matrix. Thus, the *Si* block remains in the Im-rich domain. This type of process, even more easily envisioned when one remembers the volatility of chloroform, would account for both phases exhibiting the presence of silicon.

Another viable explanation for *Si* being (apparently) present in both phases is the concept of a thin silicon-rich layer forming at the copolymer-air interface, which has been reported by others[48] for different *SiIm* block copolymers. Such a layer would form to minimize the free energy of the copolymer system and would account for the silicon being observed at the top of both phases. However, even if this layer was responsible for some of the *Si* being detected, the nature of both phases could still be determined by considering the silicon composition induced by this layer as background noise. In this case, silicon remains prevalent in the matrix region. The most reasonable explanation of the observed phase separation is more than likely a combination of these two factors -- the formation of a silicon layer *and* incomplete phase separation. In any of these three cases, though, the qualitative result remains the same: the matrix is siloxane-rich and is expected to have rubbery characteristics, while the domains are imide-rich and are expected to behave as glassy fillers.

Thermal Dynamics

Differential scanning calorimetry traces of the GE1 sample, an example of which is presented in Fig. 12, demonstrated a T_g near 227° C. This T_g was completely reproducible upon recycling the sample. In view of the reported[38] T_g for ULTEM-1000 being 215-225° C, we may conclude that the structure in Fig. 2 represents the imide block in GE1. The absence of any lower T_g (down to 25° C) suggests that the siloxane block is PDMS. The presence of a pure-imide T_g shows that *microphase* separation occurs very effectively (almost completely), even though it cannot be seen at the size scale of Figs. 6 and 8, and supports the concept of a silicon-rich layer existing on the surface of the thin films. In the case of the ultrathin films, a surface layer of *Si* would certainly explain the apparent detection of *Si* in both phases; however, the possibility of incomplete phase separation must not be ruled out in light of the earlier discussion on rapid solvent removal.

The recorded T_g for the MT3 copolymer was much lower, approximately 61° C, and was also reproducible upon recycling, as seen in Fig. 13. This T_g, too, was in agreement with the T_g reported for the copolymer by the manufacturer[35] (50-58° C). There are two possible explanations for this value. One is that $T_g \approx 60°$ C represents a blend property, such as an average lying between the high imide value (e.g., 227° C for GE1) and the low siloxane value (e.g., -120° C for PDMS[49] used in GE1). However, this could only be true for a well-mixed blend, and Fig. 4 clearly shows phase separation. The second explanation is that $T_g \approx 60°$ C represents the siloxane phase alone, in which case that material is identified as polydiphenylsiloxane (*PDPS*), which has $T_g = 62°$ C.[49] According to the supplier,[36] the siloxane is *not PDPS*, thereby indicating that the presence of the diamine, which is invisible in the TEM micrographs, substantially alters the moiety of the siloxane. The lack of a higher T_g for the imide microphase indicates it is higher than the decomposition temperature, discussed below.

Applications of *SiIm* copolymers depend on their thermal decomposition temperatures as

well as on T_g and curing temperatures. As seen in Fig. 14, thermal decomposition of well-cured MT3 is evident beyond 300° C, where the trace indicates the start of an endothermic rise. The reported[35] decomposition temperature is 350° C.

The microstructural response of partially-cured MT3 to temperature, investigated in detail elsewhere,[50] is presented in Fig. 15. Unlike the microstructures in the well-cured system, these dispersed microstructures were obtained by heating the MT3 ultrathin film in the electron microscope (with beam turned off) for 15 minutes at 324.5° C. The fact that film thickness, especially in ultrathin films, has a major impact on thermal processes and stability -- e.g., spinodal decomposition -- is well established;[41] however, the evidence that the siloxane microstructures are responding to an elevated temperature by appearing to coagulate is explicit. The appearance of regions having a significantly higher volume fraction of siloxane domains occurs only above 300° C,[50] suggesting that the relationship between the domains and matrix is being altered at or above this temperature. One reasonable explanation is that the hard imide matrix is either decomposing (Fig. 14) or becoming soluble in the soft segment. In either case, the biphasic nature of MT3 (characterized by the siloxane-diamine soft segment and the imide hard block) ceases, except for the siloxane *miniphases* caused by phase incompatibility between the siloxane and diamine blocks within the soft segment. Viscoelastic properties measured at 300° C (see below) seem to substantiate liquid-like behavior in the sense of no interconnected structure. The remaining siloxane domains can then attempt to coalesce (as in Fig. 15), since the matrix is now completely soft.

Mechanical Dynamics

I. Microstructural deformation. Relating macroscopic mechanical properties to the deformation of microstructures is a desirable goal, but for this purpose the latter should probably not be studied in the context of ultrathin films. Just as with the thermal response of an ultrathin film, the mechanical response of such a film to a strain is also going to contain artifacts related to the film thick-

ness.[41] For example, Boehme and Cargill[51] have shown that anisotropy in a polyimide film, which influences such material properties as the ultimate strength and elongation, increases as the film thickness decreases. Similar findings are evident in the GE1 optical micrographs shown in Fig. 5, where anisotropy is clearly evident in the thinnest film (cast from the 0.5% chloroform solution) and also in the TEM micrograph of Fig. 6. These problems can be minimized by using high-voltage electron microscopy (HVEM), which permits studying thicker films (e.g., 200 nm) and thereby reducing artifacts.

Tensile straining of MT3 thin films (approximately 200 nm thick) at ambient temperature and an elongation rate of 0.11-0.13 μm/sec led to the deformation of microstructures as shown in Fig. 16. At time τ=0, the domains are seen undeformed (Fig. 16a). After eight minutes of steadily increasing elongation, the microstructures become distinctly ellipsoidal (Fig. 16b); and after 21 minutes, the discrete domains have been transformed into continuous striated structures (Fig. 16c). The mechanical response of the polymer chains to the strain is shown schematically in Fig. 17, where the imide matrix is shown as the cross-hatched region and the diamine and siloxane portions of the soft segment are presented as the blank (white) and blackened regions, respectively. A multiblock copolymer can interconnect, in principle, the same number of domains as the number of those blocks in the copolymer molecule. However, due to kinetic limitations and looping effects (wherein the molecule retraces itself to place a second block in a domain), the number of interconnected domains is expected to be less than the actual number of these blocks. This latter case is shown in Fig. 17a, where the complexity of interconnected domains under no strain is somewhat simplified to illustrate the mechanism by which the continuous striations form. As the glassy or possibly crystalline[50] polyimide matrix distorts due to the strain, the rubbery siloxane domains also readily deform, but they do remain interconnected. The soft-segment blocks can accommodate this deformation to the extent that the blocks do not overextend and break. Before this break occurs, the rigid imide matrix will crack, permitting the domains themselves to be pulled into alignment

along the axis of strain (Fig. 17b). Continued deformation of the domains occurs with constant straining, and deformed domains from various thicknesses within the copolymer film seem to overlap each other (in projection), thereby appearing to be a continuous, although disordered, lamellar structure. Similar modes of deformation have been reported by Desper *et al.*,[52] who used SAXS to study the response of microstructures of various polyurethanes to tensile strain. They found that the microstructures simultaneously exhibited shear deformation, tensile deformation, and rotation/translation.

When the MT3 film is strained even further than in Fig. 16c, crazes begin to form, an example of which is presented in Fig. 18. The crazes, crack-like defects which are still load-bearing due to remaining fibrils,[53] are found to be oriented normal to the axis of strain. This is in agreement with the HVEM work of Michler,[54] who studied mechanical microprocesses in several high-impact polymers. In addition, closer examination of Fig. 18 reveals that the continuous striations appear on both sides of the craze, indicating that the craze occurred only after the microstructures had absorbed a sufficient amount of strain energy.

Since the GE1 copolymer has a rubbery matrix and a glassy domain structure (remembering that phase separation is *not* 100% complete), the response of this copolymer is expected to be very different from the MT3 copolymer. Since the GE1 matrix is primarily rubbery, tensile strain will readily deform the matrix; however, despite matrix distortion, the domains will resist deformation. The micrograph in Fig. 19, taken at 25° C and under the same strain conditions as the MT3 copolymer in Fig. 16c (i.e., 0.11-0.13 μm/sec and τ=21 minutes), clearly illustrates this deformation resistance. Even after 21 minutes of strain, the domains, although deformed, remain discrete. As in Fig. 17 for MT3, the microstructures in the GE1 copolymer are expected to deform and then align due to the rubbery matrix. Once again, the chains within the domains are extended due to the imposed strain; however, the extent to which these chains extend is inhibited by the glassy nature of the domains. Before such great extension can occur, the forces on individual glassy-block

chains can apparently build up high enough to pull these chains from their domains under continued strain.

II. Mechanical properties. Rheological studies were conducted on the MT3 copolymer only. In the first set of studies, tensile stress-strain relationships of both the fully and partially cured copolymer were investigated under ambient conditions at a constant strain rate of 2.54 mm/sec. Sample films, each measuring 0.508 mm in thickness, were obtained by casting the as-received 25% solution onto a Teflon sheet. After being cured in dry nitrogen, films having no visible blemishes were trimmed to form rectangular strips, approximately 2.0 cm long and 0.5-3.0 cm wide, which were used to determine the copolymer's stress-strain properties. For the engineering stress σ,

$$\sigma(\tau) = \frac{F(\tau)}{A_o} \tag{4}$$

where $F(\tau)$ is the force imposed as a function of time τ, and A_o is the initial cross-sectional area of the sample. The strain is given by

$$\gamma(\tau) = \frac{\delta l(\tau)}{l_o} \tag{5}$$

where l_o is the original sample length and $\delta l(\tau)$ is the displacement as a function of time.

The mechanical properties of the partially cured copolymer (cured to 120° C, only) are presented in Fig. 20. These two samples reached their maximum stress when γ=0.15 and 0.40, and their $\sigma(\gamma)$ curves are not close together. However, they share the feature of failure shortly after the peak stress, and the peak stresses are quite close in magnitude. The average of those peaks is 12.5 MPa, which matches the reported[35] yield stress (σ_y) for the fully-cured copolymer.

In the fully cured sample (cured to 200° C), the copolymer behaved much differently, as seen in Fig. 21. The initial segment of the curve represents the actual elastic strain process, identical for the two samples, and ending when yield occurs at γ=0.08 for one sample and ≈0.13 for another, with an average yield tensile stress of 12.4 MPa. This is followed by an extended draw

region (where necking was observed). Each test was terminated when the stress increased again, around $\sigma \approx 10.7\text{-}11.7$ MPa, and the crosshead was returned to its origin (with the premature zero-load strains indicating the extent of "set" -- i.e., plastic flow due to necking). No cracking was observed in these samples. The ultimate tensile stress was also determined for one fully cured sample by straining the sample until it tore apart. We observed this stress to be 14.9 MPa, close to the reported[35] 14.4 MPa.

The major mechanical-property differences between the cured (Fig. 21) and uncured (Fig. 20) samples are the ductility and toughness -- associated with drawability, high stress after yield, and large extensions before failure -- associated with curing. Microphase separation and resulting microstructures are similar for both (although less prevalent in the partially-cured copolymer[50]), as reflected in these data by the equality of low-γ peak stresses (12.5 MPa) which presumably signal breakage of the continuous hard phase (rigid polyimide). When such breakage occurs in the uncured samples, structural continuity is entirely lost and macroscopic cracking occurs. However, cured samples apparently have another mechanism to support a load when the imide continuity fails. It may be that curing induces some continuity in the soft (siloxane-rich) phase -- which may or may not involve continuity of siloxane chains -- or may crosslink it, so it can better support a load.

DMT studies of the partially cured MT3, conducted at 150° C and above, revealed time-dependent upward drifts in G' and G''. This drift, surely caused by continued curing, approached modulus values of the fully-cured polymer if allowed to proceed long enough. Behavior of the fully-cured sample is given in Fig. 22 (G') and Fig. 23 (G''). These curves were entirely stable with time and also strain-independent up to the highest strain amplitude used (2%).

Interpretation of the rheology at these temperatures is handicapped by not knowing the microstructure, which was determined only near room temperature. However, we know that T_g (≈

61° C) cannot represent the glass transition of a homogeneous system, or else the structure at lower temperature could not form. Thus, the microphase separation temperature, T_s, must exceed at least 61° C. Since, according to Leary-Henderson-Williams theory,[45,55] we have $T_s \propto (\delta_{Si} - \delta_{Im})^2$ and $\delta_{Im} >> \delta_{Si}$, we can expect that two-phase behavior can persist to quite high temperatures. One mitigating factor, possibly, is the short length of individual siloxane units; the absence of a theory for (short) multiblock copolymer microphase separation prevents evaluation of this factor.

There seems some rheological evidence of the persistence of multiphase behavior to at least 150° C. Figures 22 and 23 show that $G'(\omega)$ and $G''(\omega)$ are almost flat over a wide range of ω -- three orders of magnitude -- and have rather high values. The high values could reflect the glassy/crystalline matrix with a dispersed rubbery phase, together with an interconnectedness of domains contributed by participating molecules. The near-independence of ω is characteristic of entangled systems of very high molecular weight homopolymers and, analogously, interconnected block copolymer domain systems. Furthermore, a limiting value of G' at low ω is found for all solid-like systems (e.g., crosslinked rubber) and Fig. 22 comes close to this at 150° C.

However, such evidence dissipates at higher temperatures, and at 300° C the rheology is comparable to that expected of homogeneous systems. For example, the slope of $G'(\omega)$ at ω=0.1 s^{-1} is about 1.43 and apparently decreasing at lower ω; this is very similar to the behavior of homogeneous fluids, all of which must approach a slope of 2.00 but rarely reach it within experimental conditions (1.5 is very common). Figure 23 gives, at 300° C, a low-ω $G''(\omega)$ slope of 0.91, close to the theoretical value 1.00 for homogeneous liquids.

Attempts to assemble master curves of $G'(\omega a_T)T_R/T$ and $G''(\omega a_T)T_R/T$ using the time-temperature equivalence principle[56] (TTEP) are shown in Fig. 24. Reasonably good superposition is achieved in Fig. 24, which uses 300° C as the reference temperature (T_R). The linear relationship between log a_T and T (given in equation form in Fig. 24) does not suggest that any transition

(e.g., T_s) is taking place in this temperature range, but there are not really enough points to be sure. The DSC data in Fig. 14 exhibit enough undulation to allow such initial interpretation, but micrographs[50] such as the one obtained at 324.5° C (Fig. 15) provide evidence that microstructures, although markedly different from those seen at lower temperatures (Fig. 4), do persist up to the decomposition temperature in the MT3 copolymer.

In addition, using the rheological criterion proposed by Han and Kim[57] to determine the microphase-separation temperature in diblock and triblock copolymers, we have constructed a log G' *versus* log G'' plot (Fig. 25) to ascertain the presence of a thermally-induced phase transition. The curves corresponding to temperatures between 150° C and 250° C exhibit an inflection, which is not characteristic of a homogeneous polymer. The higher-temperature curve (300° C) does not possess this characteristic, suggesting that the anomalous behavior observed at lower temperatures is no longer present. If this inflection represents some microstructural effect due to phase separation between the diamine-siloxane soft segment and the imide hard segment, then the absence of the inflection reflects the end of phase separation (due, for example, to imide decomposition or increased diamine-imide solubility).

CONCLUSIONS

Characterization of the microstructures existing in two phase-separated poly(siloxane-imide) multiblock copolymers, in addition to bulk thermal and mechanical properties, has been established. Because the development of incorporating silicone blocks in polyimides is still so recent, little work has focused on the structure-property relationships in these new multiblock, or segmented, copolymers. Using conventional (low-voltage) transmission electron microscopy, we characterized the size of these microstructures in both the MT3 and GE1 copolymers; the former having siloxane domains on the order of 5 and 16 nm in diameter and the latter having a distribution of domain sizes including some very large (order of micrometers). Energy-dispersive X-ray microanalysis

(EDX) was utilized in discerning the compositions of the phases in the GE1 sample; subsequently, we found that the matrix appeared to be rich in silicon even though the sample is only 40% siloxane by weight. Interpretation of the observed phase separation led to three possible explanations: (1) the EDX results accurately represented the copolymer, thereby indicating incomplete phase separation with $\Delta_S \approx 0.67\text{-}0.70$, (2) a silicon-rich layer existed on the surface of the film, providing evidence for silicon to be present in both phases, or (3) a reasonable combination of (1) and (2). In either of these cases, the matrix was still rich in silicon, and the dispersed domains remained imide rich.

Dynamic TEM was successfully utilized in studying both the thermal and mechanical responses of the microstructures present in the copolymers. The domains in the MT3 sample, when heated near the thermal decomposition temperature (≈ 300-350° C), changed dramatically in appearance and resembled liquid-like droplets. Responding to tensile strain in the KRATOS high-voltage electron microscope, the microstructures of both copolymers exhibited deformation: the MT3 domains elongated to form continuous striations after about 21 minutes of strain, and the GE1 domains distorted far less after the same degree of strain due to their glassy nature.

Bulk material properties were analyzed using DSC and DMT methods. Glass-transition temperatures were found for both copolymers. The T_g of the MT3 sample was about 61° C and that of the GE1 sample about 227° C (which is comparable to that of the parent polyetherimide, ULTEM-1000). Bulk mechanical properties of the MT3 copolymer at room temperature demonstrated variations with respect to the cure cycle of the sample. For samples only partially cured, the yield stress (≈ 12.4 MPa) was attained at strains under about 0.6, but the sample tore beyond this. In the fully cured samples, this stress was achieved and followed by a plastic-flow regime to strains around 1.0 without breaking. The ultimate stress, reported[35] as 14.4 MPa, was measured here at about 14.9 MPa.

Dynamic mechanical tests at elevated temperatures also showed differences between partially and fully cured MT3 samples. In the former, storage and loss moduli were unstable and increased with time, as curing proceeded during the test. In the latter, both moduli were completely reproducible at any measured temperature and were insensitive to the strain amplitude (between 1.0% and 2.0%). Application of the TTEP[56] to create master curves of $G'(\omega a_T)T_R/T$ and $G''(\omega a_T)T_R/T$ yielded good superpositioning, with $\log(a_T)$ decreasing linearly with temperature. Such superpositioning did not suggest a phase transition (e.g., T_s) between 150° and 300° C. However, an inflection in a plot of log G' *versus* log G'' for all temperatures as high as 250° C may reflect the existence of microphase separation. This inflection seemed to be absent at 300° C, suggesting that a transition (perhaps decomposition) was occurring near this temperature.

ACKNOWLEDGMENTS

The authors would like to thank L.J. Male of General Electric Co. and R. Eddelman of M&T Chemicals Inc. for the block copolymer samples, C. Schooley and D. Davis of the Electron Microscope Laboratory (University of California, Berkeley) for guidance in TEM operations, D. Ackland and C. Echer of the National Center for Electron Microscopy (Lawrence Berkeley Laboratory) for assistance in the HVEM and EDX analyses, and D. Boyington and D. Kalika for help in performing the mechanical property tests. This work was supported by the Director, Office of Energy Research, Office of Basic Energy Sciences, Materials Science Division of the U.S. Department of Energy under Contract No. DE-AC03-76SF00098.

Nomenclature

a_d	=	domain aspect ratio
a_T	=	shift factor
A_d	=	domain area
A_o	=	sample cross-sectional area
C	=	concentration
d	=	diameter
d_{eq}	=	equivalent diameter
F	=	imposed force
G'	=	dynamic storage modulus
G''	=	dynamic loss modulus
I	=	intensity
k	=	k-factor in Eq. 1
l_o	=	undeformed sample length
δl	=	length displacement
P_z	=	absorption coefficient
R	=	proprietary substituent group
t	=	film thickness
T	=	temperature
T_g	=	glass-transition temperature
T_R	=	reference temperature
T_s	=	microphase separation temperature

Greek Letters

α_o	=	X-ray incident angle

δ	=	solubility parameter
Δ_S	=	degree of phase separation
γ	=	strain
ρ	=	mass density
σ	=	stress
σ_y	=	yield stress
τ	=	time
ω	=	frequency

Subscripts/Superscripts

A ,B	=	sample identification
dom	=	domain region
Im	=	imide
mat	=	matrix region
max	=	maximum value
min	=	minimum value
Si	=	silicon/siloxane

References

1. Annighofer, F. and Gronski, W., *Makromol. Chem.*, **185**, 2213 (1984).
2. Spontak, R.J., Williams, M.C., and Schooley, C.N., *J. Mats. Sci.*, **21**, 3173 (1986).
3. Spontak, R.J., Williams, M.C., and Agard, D.A., *Polymer*, in press.
4. Spontak, R.J., Williams, M.C., and Agard, D.A., *Macromolecules*, in press.
5. Ishizu, K., Hayashi, T., and Fukutomi, T., *Makromol. Chem.*, **187**, 689 (1986).
6. Mayer, R., *Polymer*, **15**, 137 (1974).
7. Hadziioannou, G. and Skoulios, A., *Macromolecules*, **15**, 267 (1982).
8. Hashimoto, T., Shibayama, M., and Kawai, H., *Macromolecules*, **13**, 1237 (1980).
9. Hashimoto, T., Fujimura, M., and Kawai, H., *Macromolecules*, **13**, 1660 (1980).
10. Richards, R.W. and Thomason, J.L., *Polymer*, **24**, 1089 (1983).
11. Richards, R.W. and Thomason, J.L., *Macromolecules*, **16**, 982 (1983).
12. Bates, F.S., Dierker, S.B., and Wignall, G.D., *Macromolecules*, **19**, 1938 (1986).
13. Hashimoto, T., Tsukahara, Y., Tachi, K., and Kawai, H., *Macromolecules*, **16**, 648 (1983).
14. Diamant, J., Soong, D.S., and Williams, M.C., in *Contemporary Topics in Polymer Science*, W.J. Bailey and T. Tsurata, eds., Plenum Press, New York, 1984, Vol. 4.
15. Annighofer, F. and Gronski, W., *Colloid & Polym. Sci.*, **261**, 15 (1983).
16. Diamant, J., *Ph.D. Thesis*, University of California, Berkeley, 1982.
17. Camberlin, Y. and Pascault, J.P., *J. Polym. Sci., Polym. Phys. Ed.*, **22**, 1835 (1984).
18. Pascault, J.P. and Camberlin, Y., *Polymer Comm.*, **27**, 230 (1986).
19. Leung, L.M. and Koberstein, J.T., *Macromolecules*, **19**, 706 (1986).
20. Chee, K.K. and Farris, R.J., *J. Appl. Polym. Sci.*, **29**, 2529 (1984).
21. King, J.J. and Lee, B.H., in *High Performance Polymers: Their Origin and Development*, R.B. Seymour and G.S. Kirshenbaum, eds., Elsevier Science Publishing Co., Inc., New York, 1986, pp. 317-330.

22. Sweeting, O.J., in *The Science and Technology of Polymer Films*, O.J. Sweeting, ed., John Wiley & Sons, Inc., New York, 1971, pp. 658-667.

23. Wilson, A.M., in *Polyimides: Synthesis, Characterization, and Applications*, K.L. Mittal, ed., Plenum Press, New York, 1984, Vol. II, pp. 715-733.

24. Merrem, H.J., Klug, R., and Hartner, H., *Polyimides: Synthesis, Characterization, and Applications*, K.L. Mittal, ed., Plenum Press, New York, 1984, Vol. II, pp. 919-931.

25. Pariser, R., *Polym. J.*, **19**, 127 (1987).

26. Kowell, S.T., Selfridge, R., Eldering, C., Matloff, N., Stroeve, P., Higgins, B., Srinivasan, M.P., and Coleman, L.B., submitted to *Thin Solid Films*.

27. Babu, G.N., in *Polyimides: Synthesis, Characterization, and Applications*, K.L. Mittal, ed., Plenum Press, New York, 1984, Vol. I, pp. 51-65.

28. Wirth, J.G., in *High Performance Polymers: Their Origin and Development*, R.B. Seymour and G.S. Kirshenbaum, eds., Elsevier Science Publishing Co., Inc., New York, 1986, pp. 195-205.

29. Serfaty, I.W., in *Polyimides: Synthesis, Characterization, and Applications*, K.L. Mittal, ed., Plenum Press, New York, 1984, Vol. I, pp. 149-161.

30. Fearon, F.W.G., in *High Performance Polymers: Their Origin and Development*, R.B. Seymour and G.S. Kirshenbaum, eds., Elsevier Science Publishing Co., Inc., New York, 1986, pp. 381-388.

31. Melliar-Smith, C.M., Matsuoka, S., and Hubbauer, P., *Plastics and Rubber: Materials and Applications*, **5**, 49 (1980).

32. Berger, A., U.S. Patent 4,139,547 (1979).

33. Berger, A., U.S. Patent 4,395,527 (1983).

34. Berger, A., in *Polyimides: Synthesis, Characterization, and Applications*, K.L. Mittal, ed., Plenum Press, New York, 1984, Vol. I, pp. 67-75.

35. M&T 3500 Siloxane Polyimide Data Sheet, M&T Chemicals, Rahway, New Jersey, 1983.

36. Eddelman, R., M&T Chemicals, Inc., personal communications, 1987.

37. Male, J. and Floryan D., General Electric Co., personal communications, 1987.

38. Spontak, R.J., in *Proceedings of the 44th Annual Meeting of the Electron Microscopy Society of America*, G.W. Bailey, ed., San Francisco Press Inc., San Francisco, 1986, pp. 788-789.

39. User's Guide, National Center for Electron Microscopy, Lawrence Berkeley Laboratory, Publication 475, 1987.

40. Delly, J.G., *Photography through the Microscope*, Eastman Kodak, Rochester, New York, 1980, pp. 66-67.

41. Butler, E.P. and Hale, K.F., in *Practical Methods in Electron Microscopy*, A.M. Glauert, ed., North-Holland Publishing Co., Amsterdam, 1981, Vol. 9.

42. Vaughan, D., *Energy-dispersive X-ray Microanalysis: An Introduction*, Kevex Corporation, Foster City, California, 1983.

43. Williams, D.B., *Practical Analytical Electron Microscopy in Materials Science*, Philips Electronic Instruments Inc., Mahwah, New Jersey, 1984, Chap. 4.

44. Xie, M. and Camberlin, Y., *Makromol. Chem.*, **187**, 383 (1986).

45. Leary, D.F. and Williams, M.C., *J. Polym. Sci., Polym. Phys. Ed.*, **11**, 345 (1973).

46. Spontak, R.J. and Williams, M.C., in *Proceedings of the Pacific Workshop on Phase Transformations*, San Francisco Press Inc., San Francisco, in press.

47. Miller, J.A., Pruckmayr, G., Epperson, E., and Cooper, S.L., *Polymer*, **26**, 1915 (1985).

48. Arnold, C.A., Summers, J.D., Bott, R.H., Taylor, L.T., Ward, T.C., and McGrath, J.E., in *Proceedings of the Society for Advancement of Materials and Process Engineering*, April 1987.

49. Brandrup, J. and Immergut, E.H., Eds., *Polymer Handbook*, Interscience, New York, 1966.

50. Spontak, R.J. and Williams, M.C., manuscript in preparation.

51. Boehme, R.F. and Cargill, G.S., in *Polyimides: Synthesis, Characterization, and Applications*, K.L. Mittal, ed., Plenum Press, New York, 1984, Vol. I, pp. 461-476.

52. Desper, C.R., Schneider, N.S., Jasinski, J.P., and Lin, J.S., *Macromolecules*, **18**, 2755 (1985).

53. Brown, H.R., *Polymer*, **26**, 483 (1985).

54. Michler, G.H. *Polymer*, **27**, 323 (1986).

55. Henderson, C.P. and Williams, M.C., *J. Polym. Sci., Polym. Phys. Ed.*, **23**, 1001 (1985).

55. van Krevelen, D.W., *Properties of Polymers: Their Estimation and Correlation with Chemical Structure*, Elsevier Scientific Publishing Company, Amsterdam, 1976, pp. 289-294.

56. Han, C.D. and Kim, J., *J. Polym. Sci., Polym. Phys. Ed.*, **25**, 1741 (1987).

Table I. Material properties of the poly(siloxane-imide) block copolymers used in this study.[a]

Property	MT3	GE1
Soft-segment content[b] (wt%)	74	40
Molecular weight (g/mol)	50,000-100,000	30,000
Block ratio[c]	1	10-15
Glass-transition temperature (° C)	50-58	-
Polydispersity index ($\overline{M}_w/\overline{M}_n$)	2.0	2.0

[a] Provided by the manufacturer.

[b] This represents the entire soft segment, including the siloxane *and* the diamine in the MT3 copolymer and the siloxane block alone in the GE1 copolymer.

[c] Defined as the number of soft segments per imide block.

Table II. Average areas and diameters of the domains formed in the GE1 copolymer as a function of casting solution (chloroform) concentration.[a]

Concentration (%)	$\bar{A}_d$ (μm^2)	$\bar{d}^b_{eq}$ (μm)	$\bar{d}^c$ (μm)
0.5	0.070	0.299	0.225
1.0	0.074	0.308	0.284
2.0	0.072	0.303	0.295
Average[d]	0.072	0.303	0.260

[a] Measurements made with a Numonics Corp. 1224 Electronic Graphics Calculator.

[b] Defined as $(4\bar{A}_d/\pi)^{1/2}$.

[c] Obtained by examining only regular domains appearing two-dimensionally circular.

[d] Found by arithmetically averaging the domain parameters from all the solution concentrations (film thicknesses).

Table III. *k*-factors used in the EDX elemental analysis.[a]

Element & Line	k-factor
C Kα	4.0000
N Kα	3.5000
O Kα	1.1500
Si Kα	1.0000
Cl Kα	1.0714

[a] Experimentally ascertained by Kevex Corporation and the National Center for Electron Microscopy.

Table IV. Domain and matrix composition results from the EDX analysis.

Absorption Corrected?	Region	Composition (%)	Elements Present[a] C	O	Si	Cl
No	Domain	Weight	62.02±3.95	16.72±0.75	19.07±2.71	2.18±1.000
		Atomic	74.25±2.75	15.05±0.93	9.80±1.63	0.89±0.43
	Matrix	Weight	42.53±0.64	18.82±0.88	38.65±1.20	0.00
		Atomic	58.11±0.57	19.30±0.81	22.58±0.86	0.00
Yes	Domain	Weight	63.83±3.26	16.62±0.76	17.51±2.30	2.04±0.90
		Atomic	75.51±2.20	14.77±0.81	8.89±1.35	0.83±0.38
	Matrix	Weight	45.60±1.03	18.73±0.98	35.66±1.68	0.00
		Atomic	60.87±0.81	18.77±0.85	20.37±1.17	0.00

[a] Nitrogen was not detected in appreciable quantities.

Figure Captions

Figure 1. Chemical structure of an SiIm copolymer, but *not* necessarily the one studied here, produced by M&T Chemicals Inc. The soft block is comprised of both diamine and siloxane segments, and the hard block is a polyimide. Substituent groups are proprietary and have not been revealed.

Figure 2. Chemical structure of the parent polyetherimide, ULTEM-1000, of the GE1 SiIm block copolymer. The ether linkages, in addition to the siloxane, afford this polyimide added flexibility.

Figure 3. Schematic diagram of the straining holder used in conjunction with the straining stage on the KRATOS 1.5MeV electron microscope. The brass plates slide along glide tracks, glued to one plate with an epoxy-phenolic adhesive. Polymer films are cast directly onto trimmed copper grids and are strained as the grids are stretched apart.

Figure 4. Electron micrograph of the MT3 copolymer taken with a JEOL JEM 100CX electron microscope. The siloxane microstructures, seen as randomly ordered dark dots, exhibit a somewhat bimodal size distribution, with a large domains being approximately 16 nm in diameter and the smaller ones about 5 nm in diameter.

Figure 5. Optical micrographs, acquired using Nomarski differential contrast spectroscopy, of the GE1 copolymer as a function of casting solution concentration (and, subsequently, film thickness). Globular stretching is observed in (a), which represents a 0.5% solution. These traces are not seen in (b) or (c), which correspond to 1.0% and 2.0% solutions, respectively.

Figure 6. Electron micrographs of the GE1 copolymers also as a function of the casting solution concentration: (a) 0.5%, (b), 1.0%, and (c) 2.0%. Distinct microstructural deformation, caused by having an ultrathin film that is thinner than the system's critical thickness, is apparent in (a) and becomes less pronounced in (b) and (c).

Figure 7. EDX elemental spectra of the domain (a) and matrix (b) of the GE1 copolymer acquired with an ultrathin window spectrometer operating at -168° C in an analytical electron microscope. The silicon peak is significantly lower in (a) than in (b), whereas the carbon peak is higher in (a) than in (b). This, along with a chlorine peak, indicative of residual chloroform solvent which is preferential for the imide block, in (a), suggests that the matrix is siloxane-rich (rubbery) and the domains are imide-rich (glassy). Peaks showing the presence of aluminum and copper are artifacts due to an aluminum holder and the copper support grid.

Figure 8. X-ray map obtained by EDX of the phase-separated GE1 copolymer. The image-enhanced region is seen in the lower right. Comparison of this region with the silicon map (upper left), the carbon map (lower left), and the chlorine map (upper right) verifies the silicon-rich matrix and carbon- and chlorine-rich domains first noticed from the spectra in Fig. 7.

Figure 9. Domain topography in the GE1 copolymer inferred from a characteristic X-ray map of the domain and matrix regions (Fig. 8). Domains thicker than the matrix appear darker in transmission. Matrix regions adjacent to the domains appear darker in TEM and produce more Si X-rays in EDX than the remaining matrix due to increasing thickness.

Figure 10. Stereo pair of electron micrographs of the GE1 copolymer. The micrographs in this pair, obtained by tilting the goniometer stage of the electron micrograph,

differ by 10° and, when viewed with a stereo viewer, offer a three-dimensional representation of the copolymer film. Domains do appear to protrude from the film, and ripples are also present.

Figure 11. X-ray trace across a domain measuring approximately 4.4 μm in diameter in the GE1 copolymer. Here, quantification of the silicon, carbon, and chlorine compositions illustrates the degree to which the matrix is silicon-rich and the domains are carbon- and chlorine-rich.

Figure 12. Differential scanning calorimetry traces of the GE1 copolymer were obtained at a heating rate of 5°/min on a Mettler FP84 DSC. Here, both the original trace and the trace obtained after recycling the film are presented. The observed T_g in the original sample was at 232° C and that in the recycled sample was 227° C. Upon analyzing several samples, including recycled samples, the average T_g was found to be 227° C.

Figure 13. DSC traces of the MT3 copolymer using the same procedure as described in Fig. 12. In both cases, the T_g remains about 60-62° C.

Figure 14. DSC trace of the MT3 copolymer acquired at a scanning rate of 10°/min and illustrating both the glass-transition phenomenon and the thermal-decomposition behavior of this copolymer at temperatures above 300° C.

Figure 15. *In-situ* observation of the microstructures in the partially cured MT3 copolymer as the ultrathin film is heated in the electron microscope to 324.5° C for 15 minutes. The sparse distribution of domains is replaced by heavily populated areas. The size distribution, too, no longer appears to be even approximately bimodal.

Figure 16. Real-time sequence of the tensile deformation of siloxane microstructures in the

MT3 copolymer. In (a), the domains are under no strain at τ=0 minutes. The rubbery domains, normally spherical, become ellipsoidal as strain proceeds for 8 minutes (b) in the direction of the arrow. Discrete microstructures yield to continuous striations after prolonged strain in (c), where τ= 21 minutes. Bar = 20 nm.

Figure 17. Schematic representation of the deformation process in the MT3 multiblock copolymer. The complexity of the chain interconnections at rest is illustrated in (a). The polyimide matrix is denoted by the cross-hatching, while the diamine and siloxane portions of the soft block are presented as the blank (white) and blackened regions. Upon initial tensile strain, the rubbery chains within the domains are elongated, thereby distorting the domains. Under continued strain, the rigid imide matrix cracks at points of stress build-up, letting the flexible block endure continued deformation (b). The siloxane domains steadily elongate due to their resiliency and align due to tension in the entire polymer molecule. Fully deformed domains found at varying levels within the film overlap (in transmission) and appear to form striations.

Figure 18. Electron micrograph of a craze within the MT3 copolymer film. Close examination reveals that the striated structure found in Fig. 17 appears on *both* sides of the craze, suggesting that the film reached its maximum stress and then crazed.

Figure 19. *In-situ* observation of the deformed domains obtained by straining the GE1 copolymer for 20.5 minutes (as in Fig. 17) in the direction of the arrow. Since these domains, unlike those in the MT3 copolymer, are glassy, tensile deformation is resisted while the rubbery matrix is distorted.

Figure 20. Bulk stress-strain curves for two partially cured MT3 copolymer samples, acquired

at a constant strain rate of 2.54 mm/sec on an MTS Hydraulic Testing Apparatus at ambient temperature. After the average yield stress (12.4 MPa) was attained, the sample tore upon further straining. Variations in the curves are due to different sample dimensions.

Figure 21. Stress-strain curves for two samples of the fully cured MT3 copolymer obtained under the same conditions as in Fig. 20. The upper portion of each curve indicates the straining process with the first peak, representing the yield stress (σ_y), occurring at an average of 12.4 MPa. After the yield stress, the samples entered into the plasticized region and then exhibited another peak ($<\sigma>\approx$ 11.1 MPa). Full recovery was observed, as indicated by the lower portion of each curve.

Figure 22. The dynamic storage modulus (G') of the MT3 copolymer as a function of frequency (ω) at four elevated temperatures (° C): 150° (●), 200° (o), 250° (▲), and 300° (Δ). G' increases with ω for a given T but decreases with temperature at constant ω, being most sensitive to temperature at the low-ω threshold.

Figure 23. G'' of the MT3 copolymer. G'' exhibits the same behavior as G' (Fig. 22), but is almost insensitive to temperature (denoted by the same symbols as in Fig. 22) at the high-ω spectrum for temperatures up to 250° C.

Figure 24. Master curves of $G'(\omega a_T)T_R/T$ and $G''(\omega a_T)T_R/T$ using the time-temperature equivalence principle[56] (TTEP). Accurate superpositioning was obtained by superpositioning both the $G'T_R/T$ and $G''T_R/T$ data simultaneously. The reference temperature (T_R) is 300° C, and the temperature symbols are the same as in Fig. 22. The logarithm of the shift factor a_T is found to be a linear function of T and is provided in equation form.

Figure 25. Plot of log G' *versus* log G'' to discern a thermally-induced phase transition, according to the method proposed by Han and Kim.[57] Persistence of an inflection in the curve up to 250° C, followed by its disappearance at 300° C, suggests the possibility of a transition (e.g., decomposition) in the MT3 copolymer.

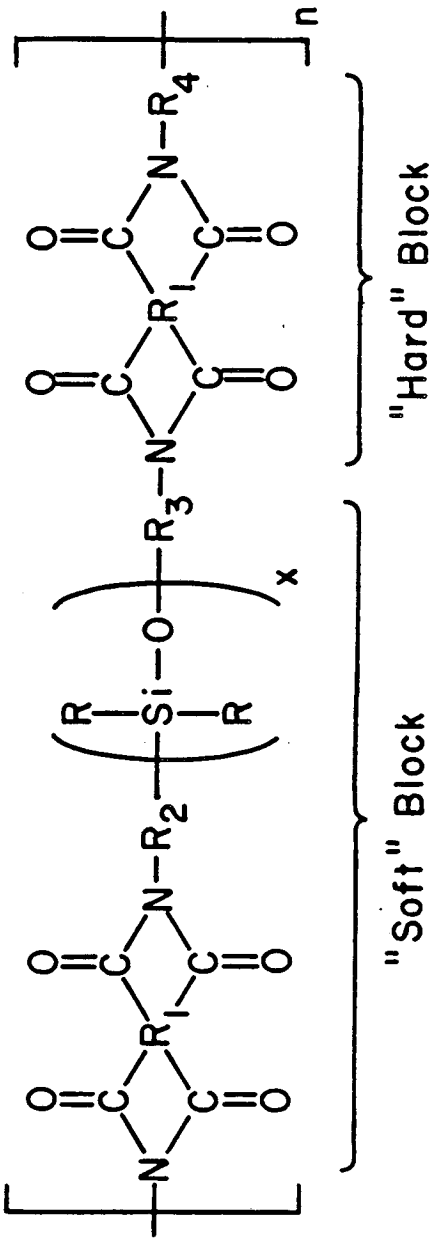

XBL 881-171

Fig. 1

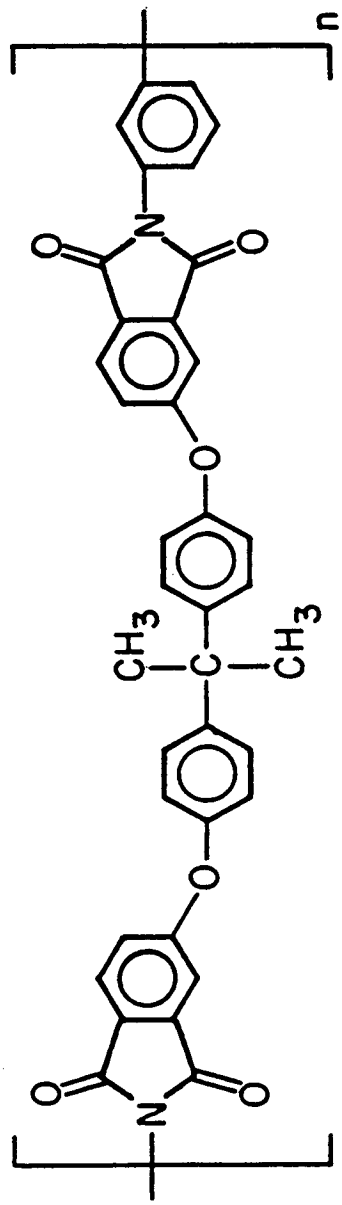

ULTEM-1000

XBL 881-169

Fig. 2

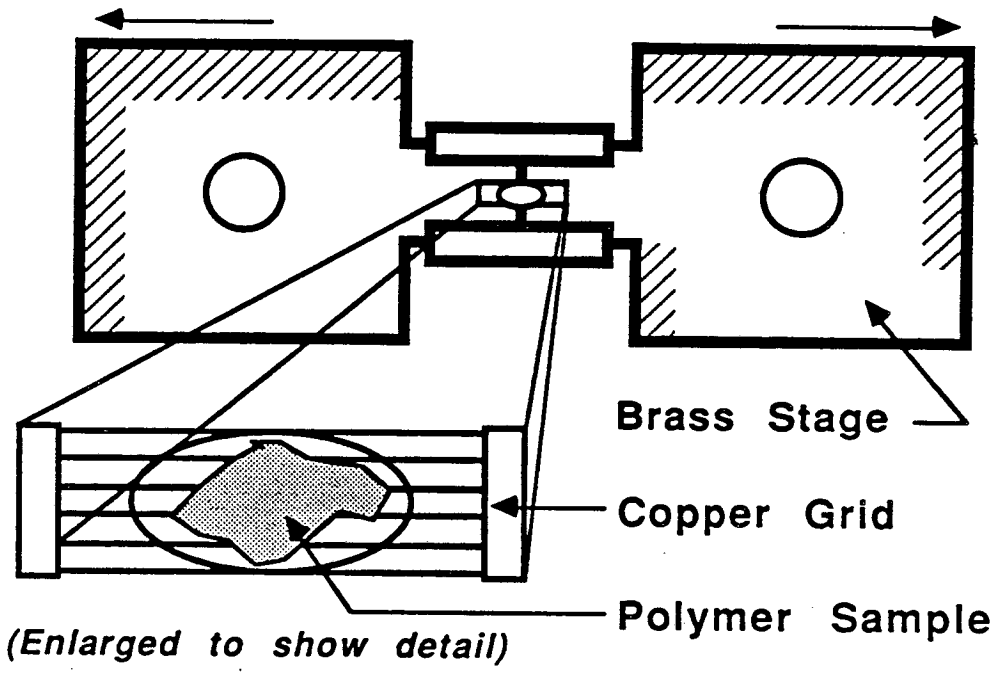

XBL 871-365

Fig. 3

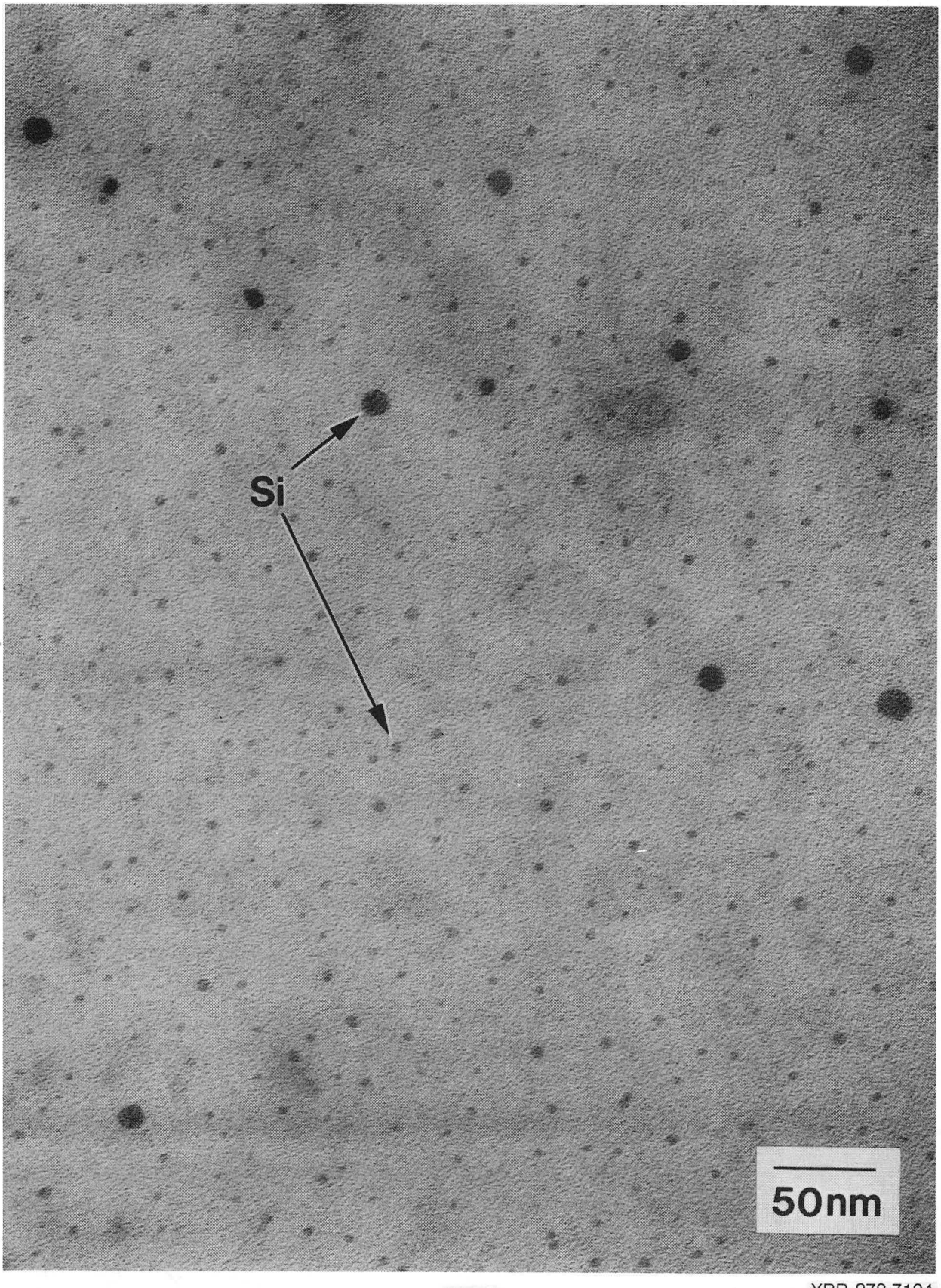

Fig. 4

XBB 878-7104

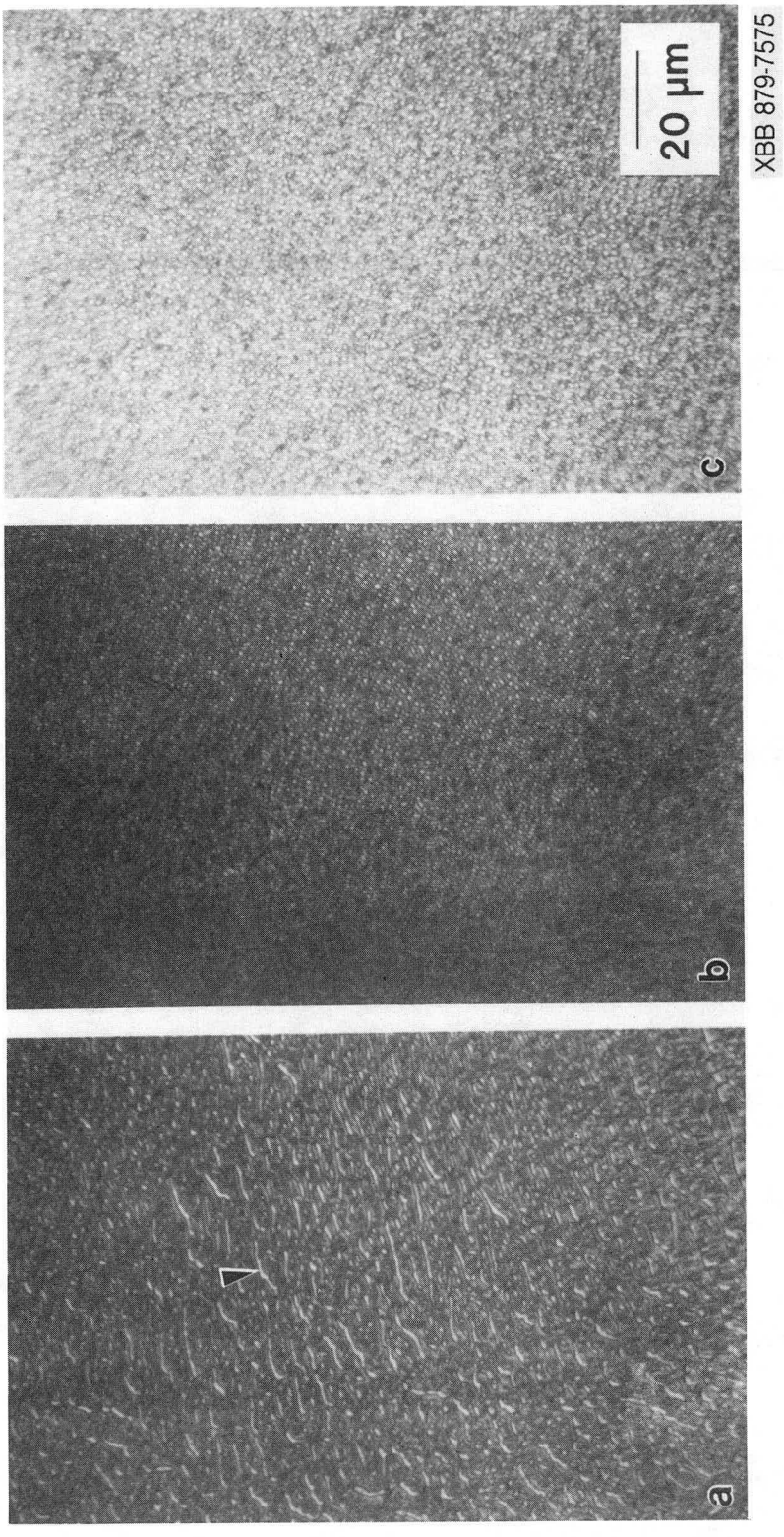

Fig. 5

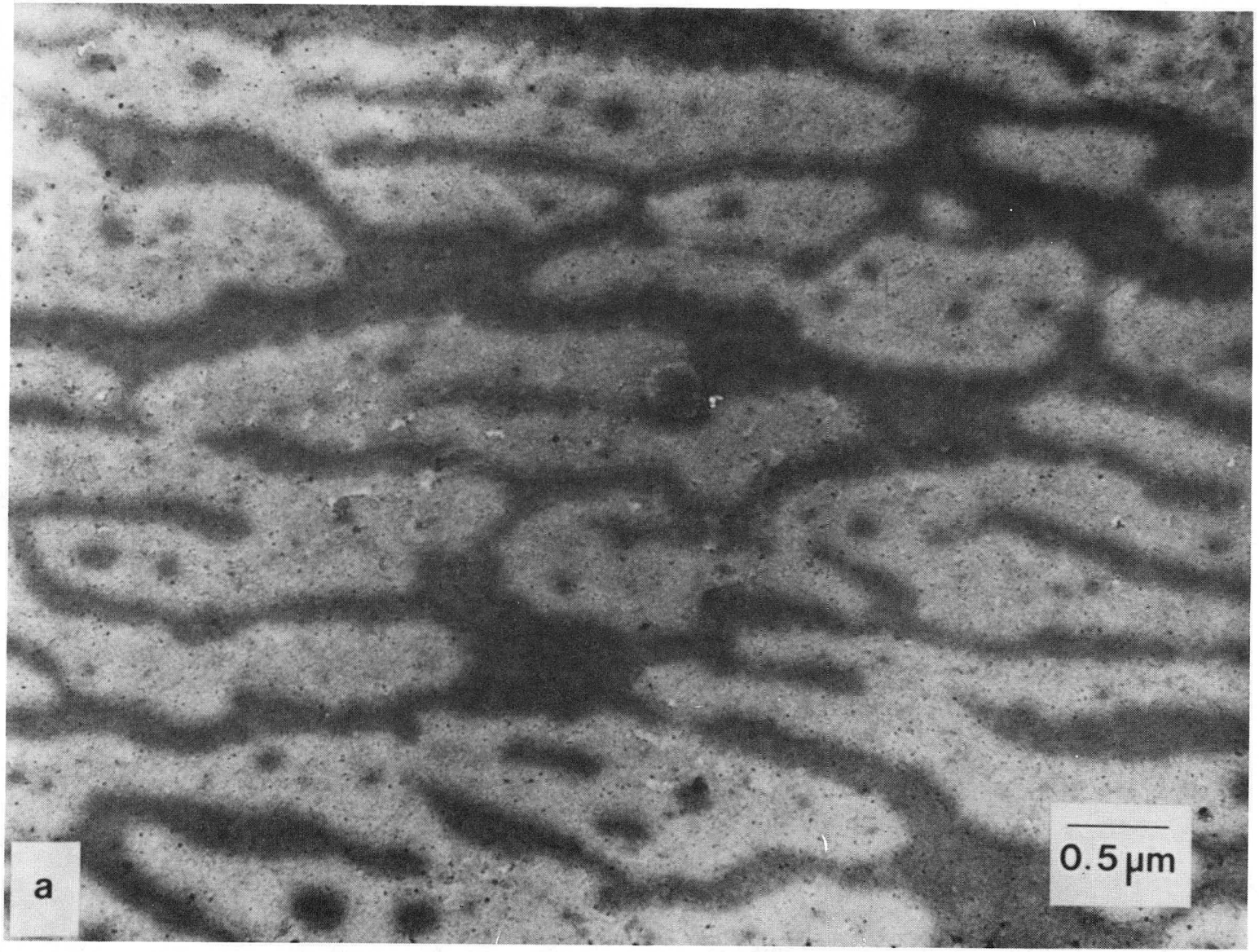

XBB 878-7101

Fig. 6a

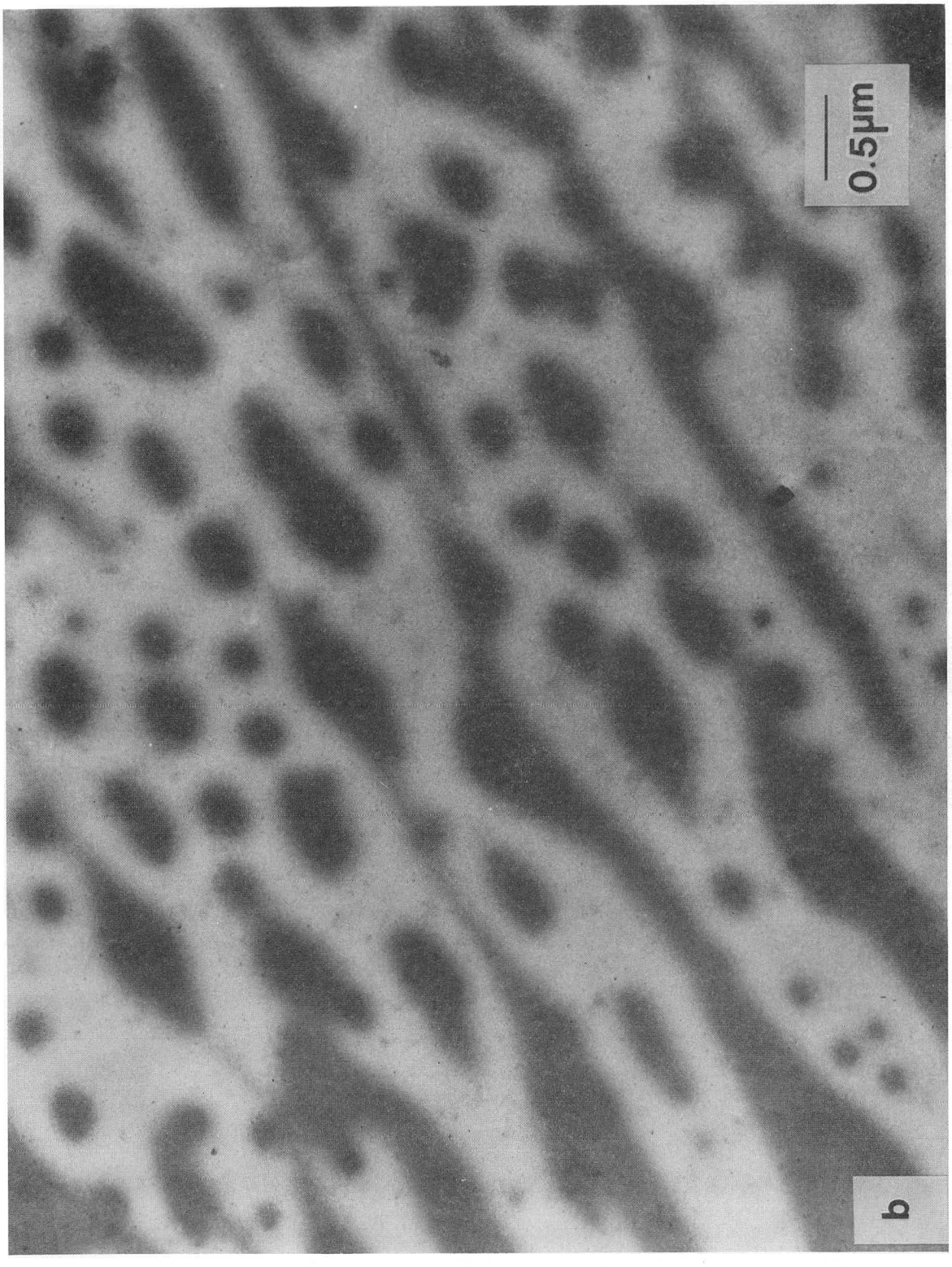

XBB 878-7102

Fig. 6b

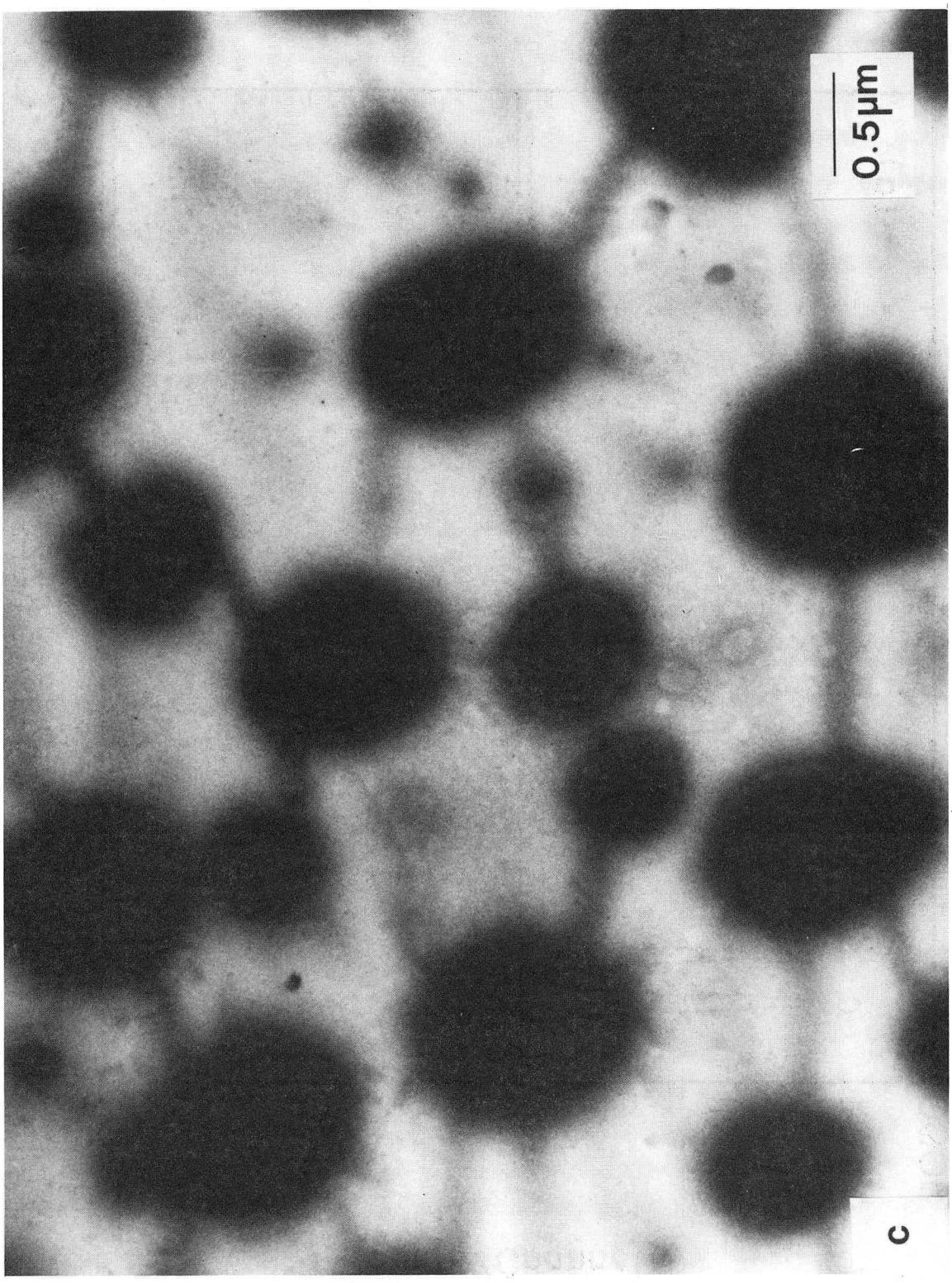

XBB 878-7103

Fig. 6c

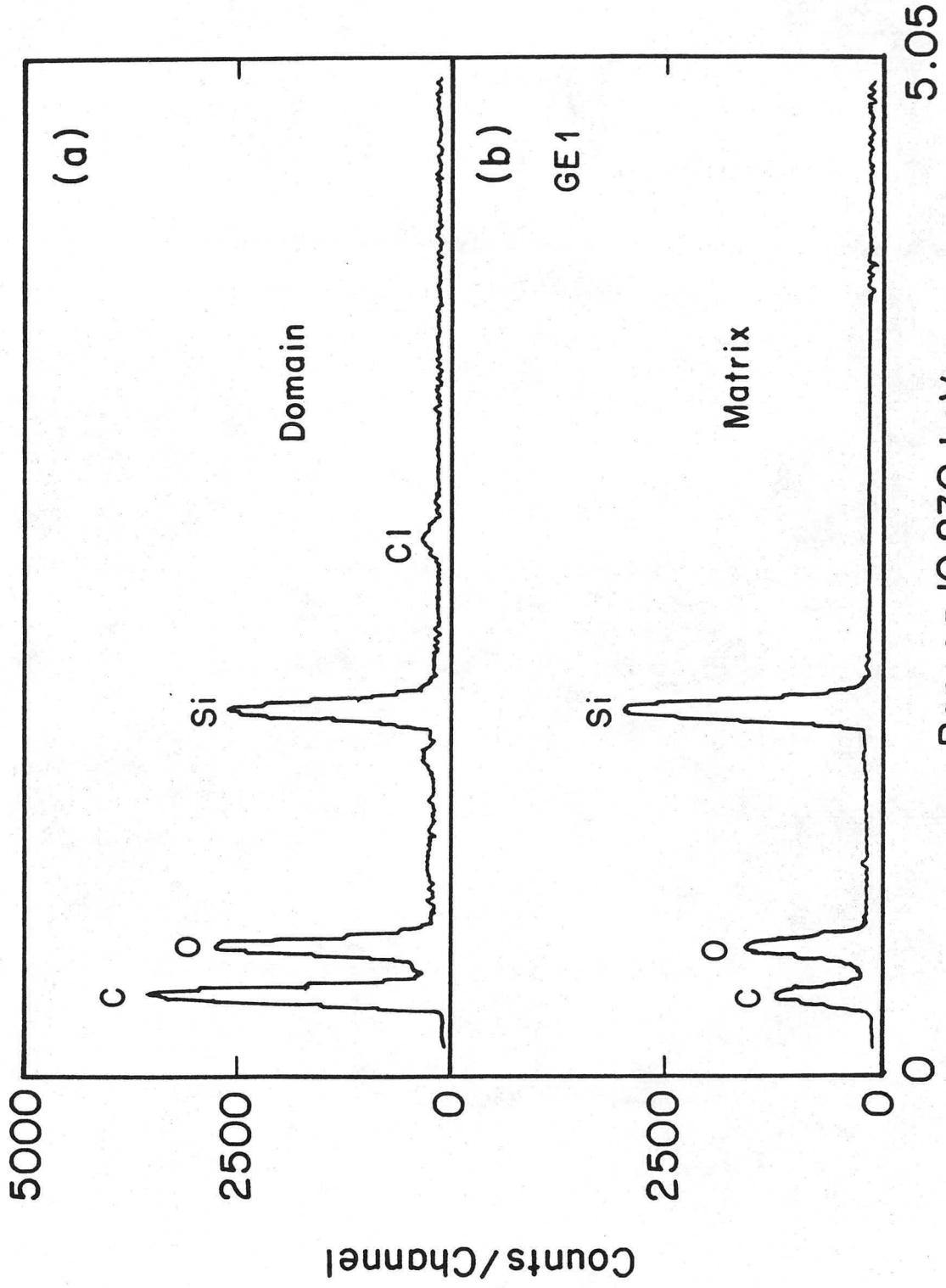

XBL 881-160

Fig. 7

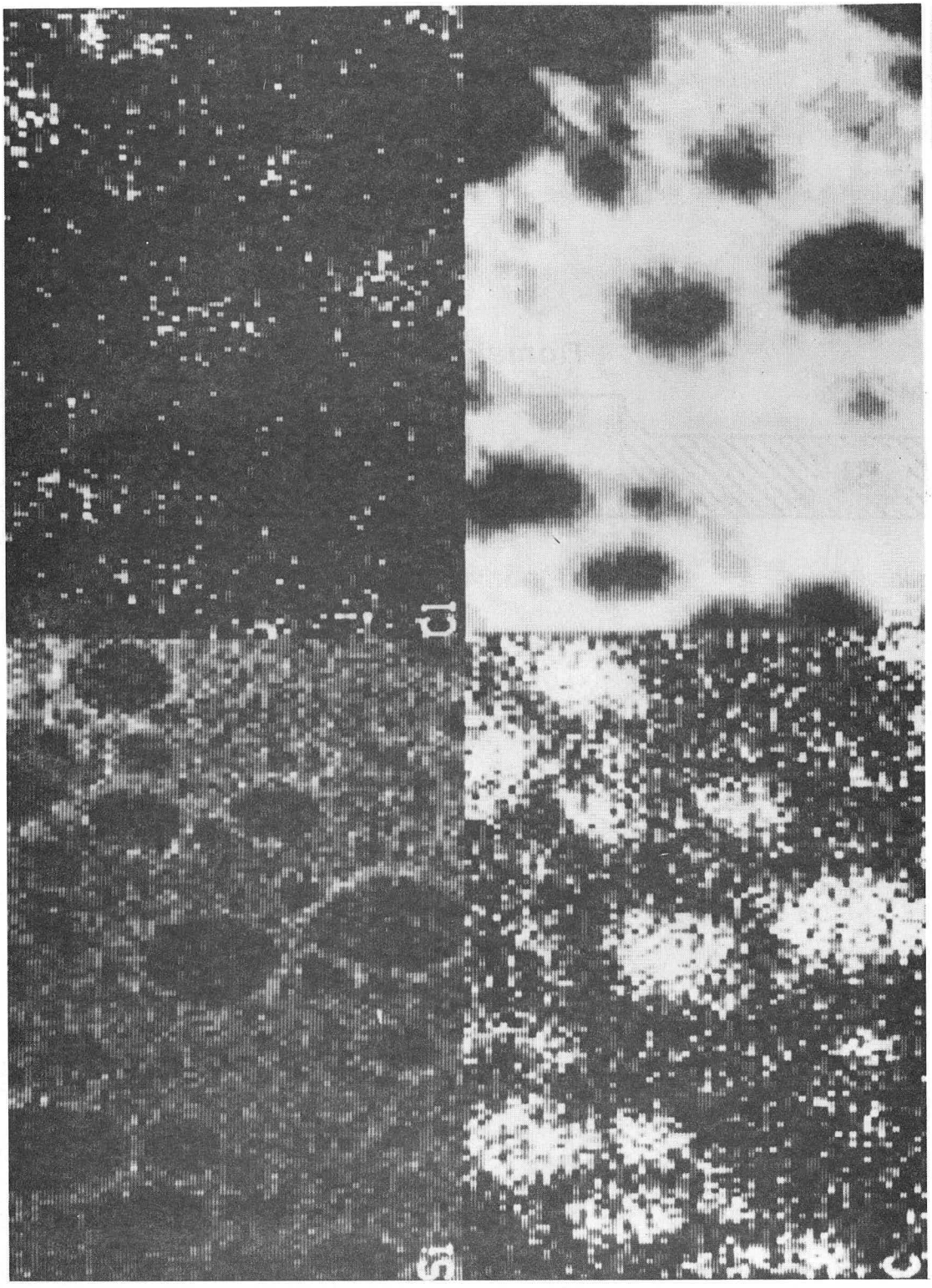

XBB 870-9761

Fig. 8

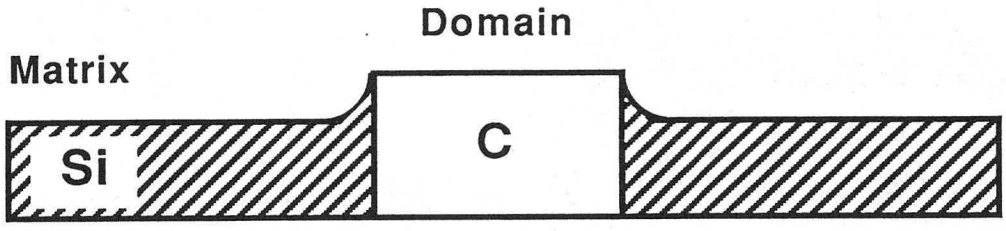

XBL 881-168

Fig. 9

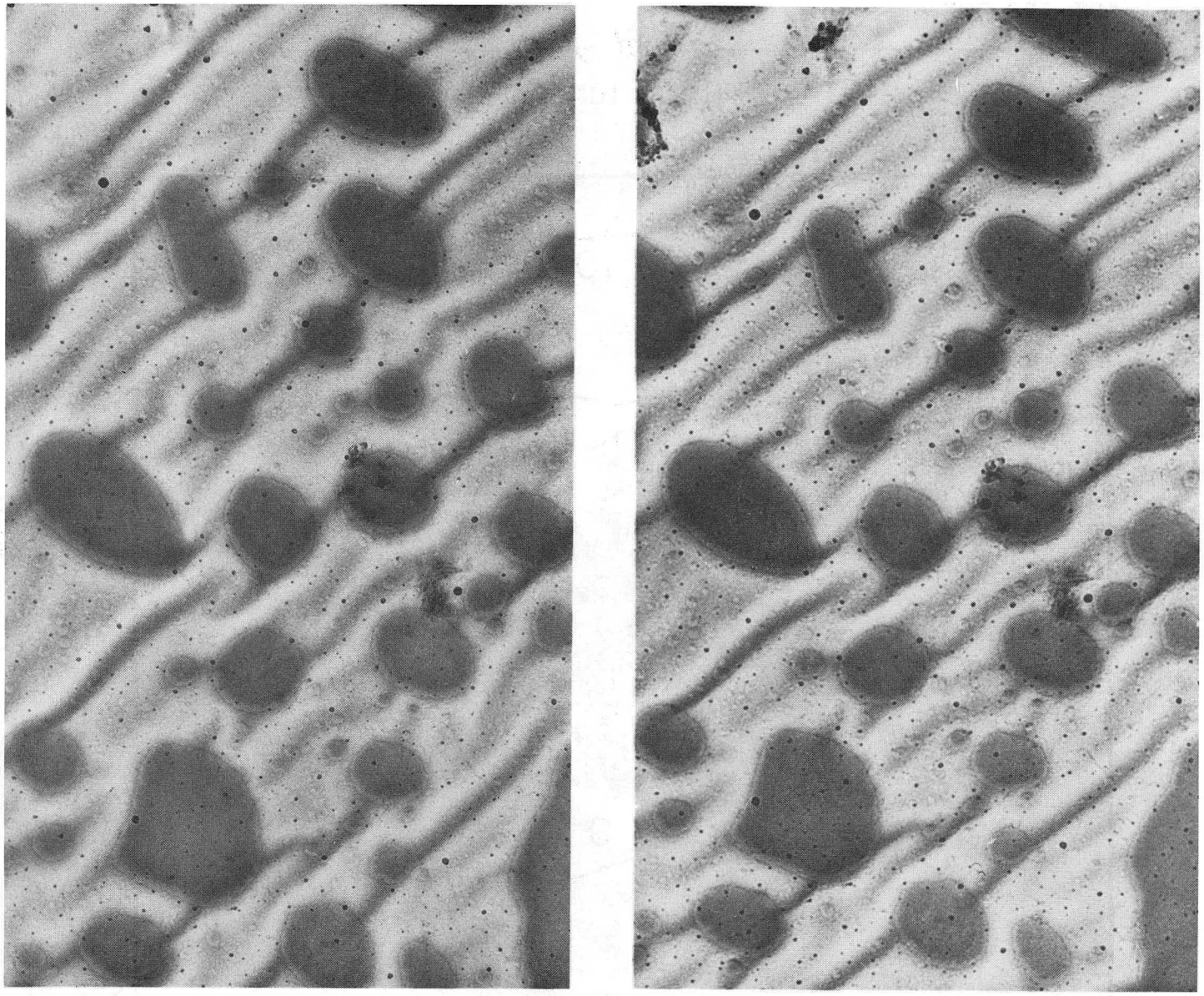

XBB 879-7576

Fig. 10

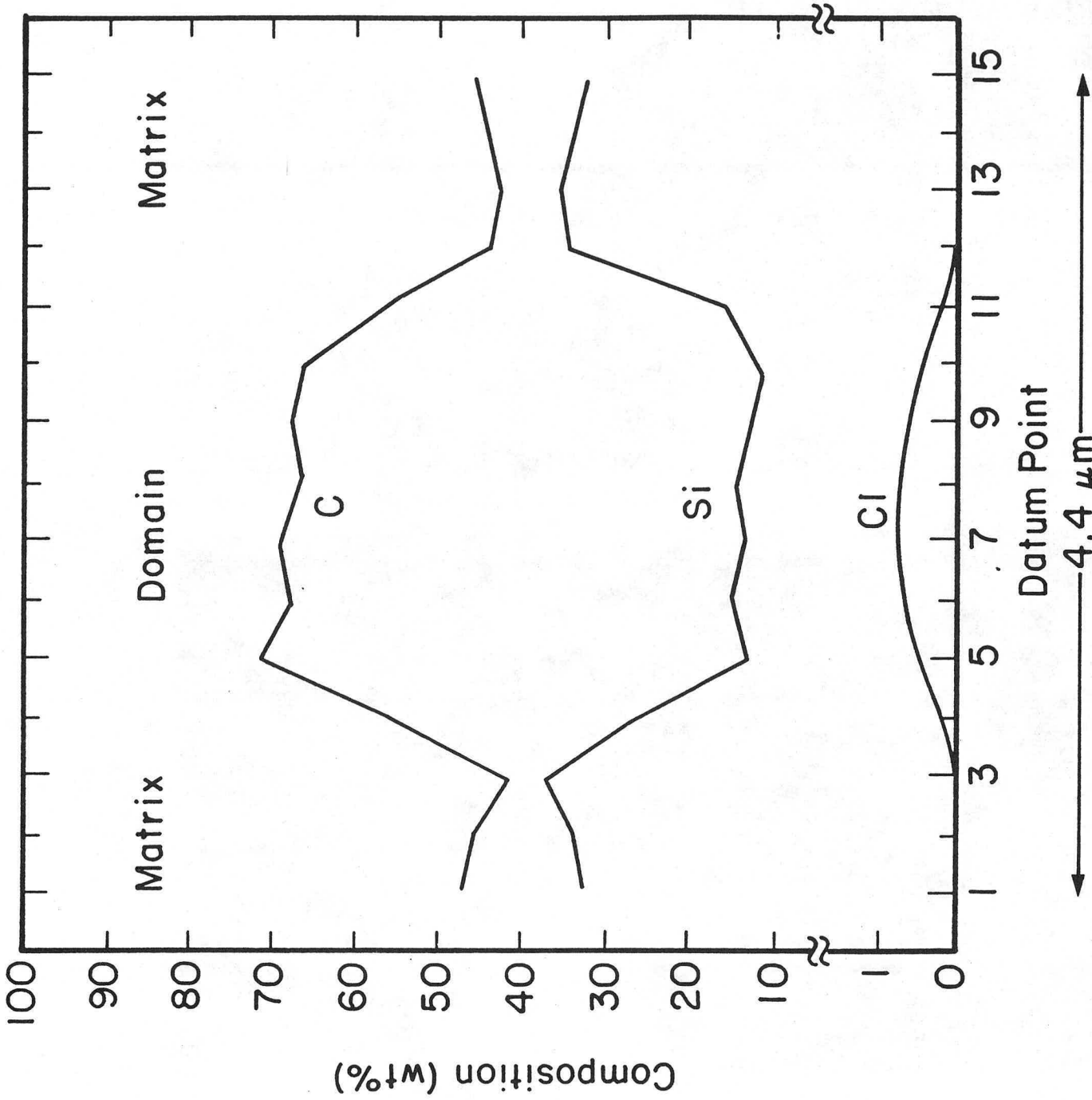
Matrix
Domain
Matrix
C
Si
Cl
Composition (wt%)
100
90
80
70
60
50
40
30
20
10
1
0
1
3
5
7
9
11
13
15
Datum Point
4.4 μm
XBL 881-167

Fig. 11

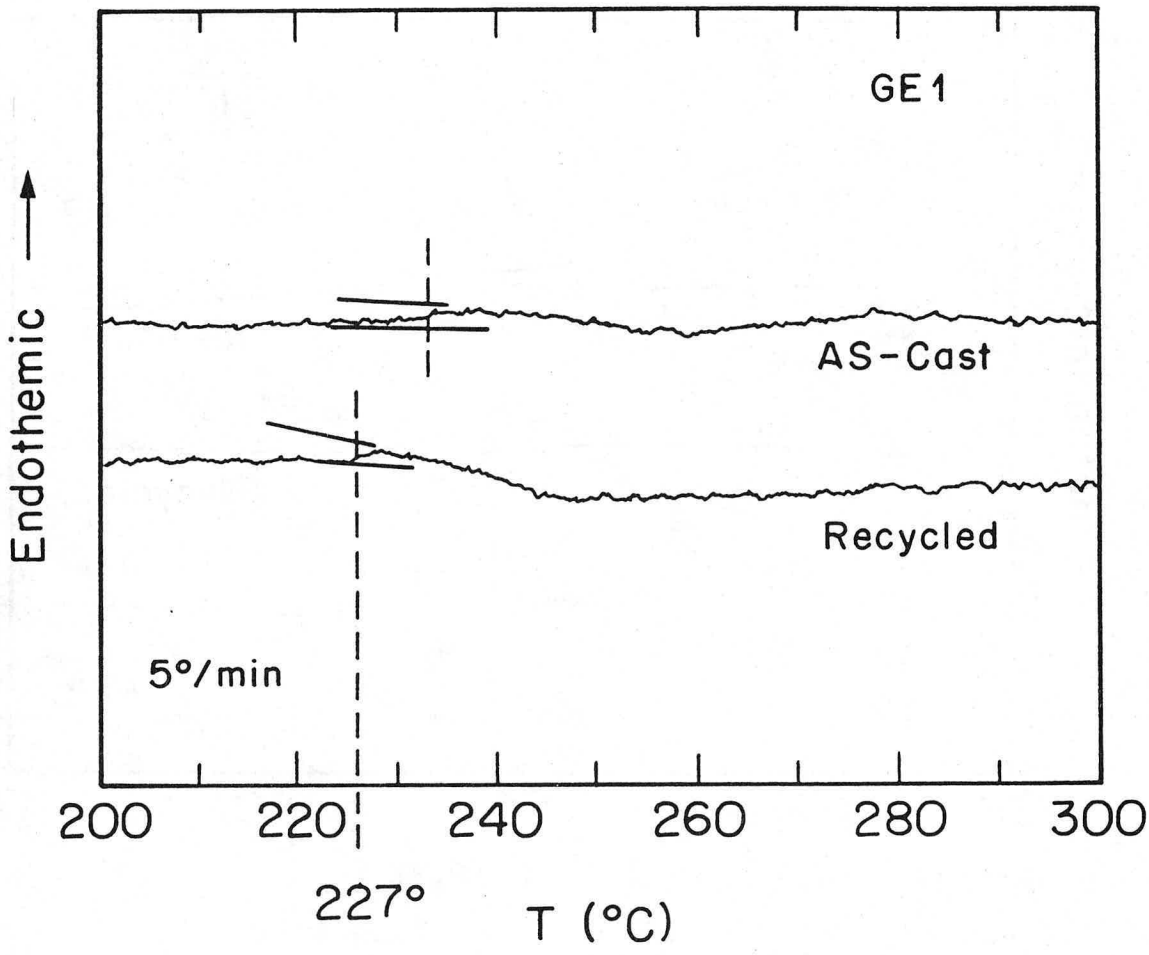

XBL 881-166

Fig. 12

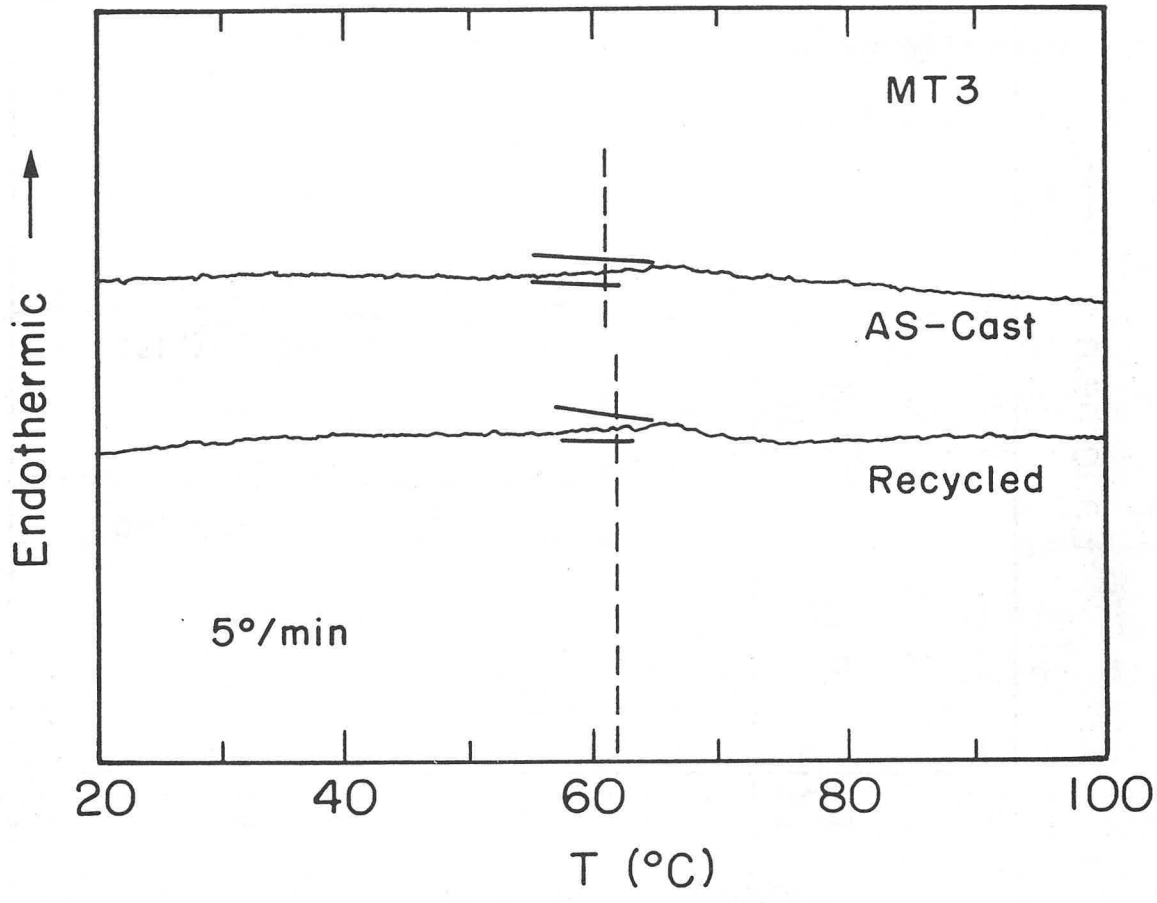

XBL 881-165

Fig. 13

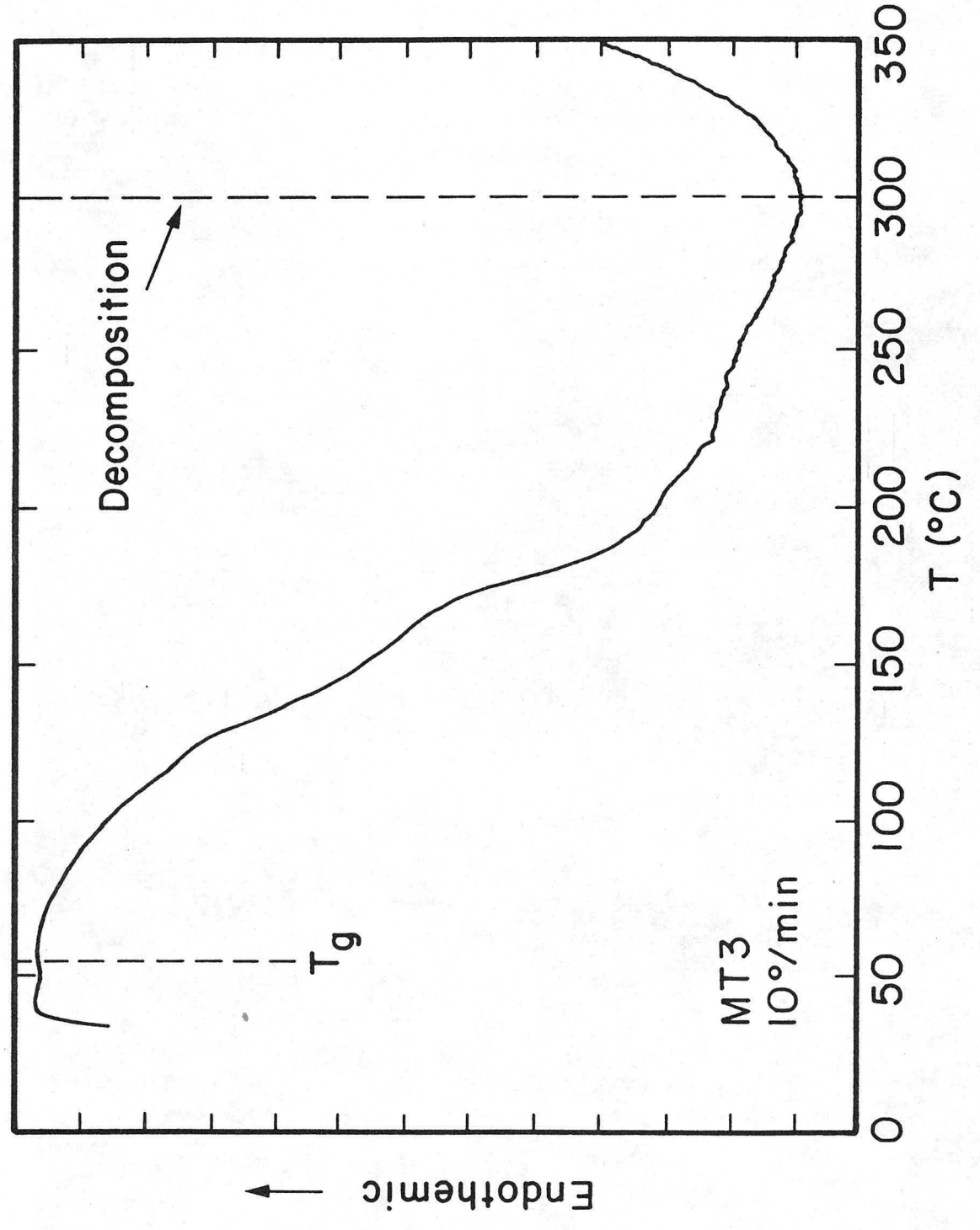

XBL 881-164

Fig. 14

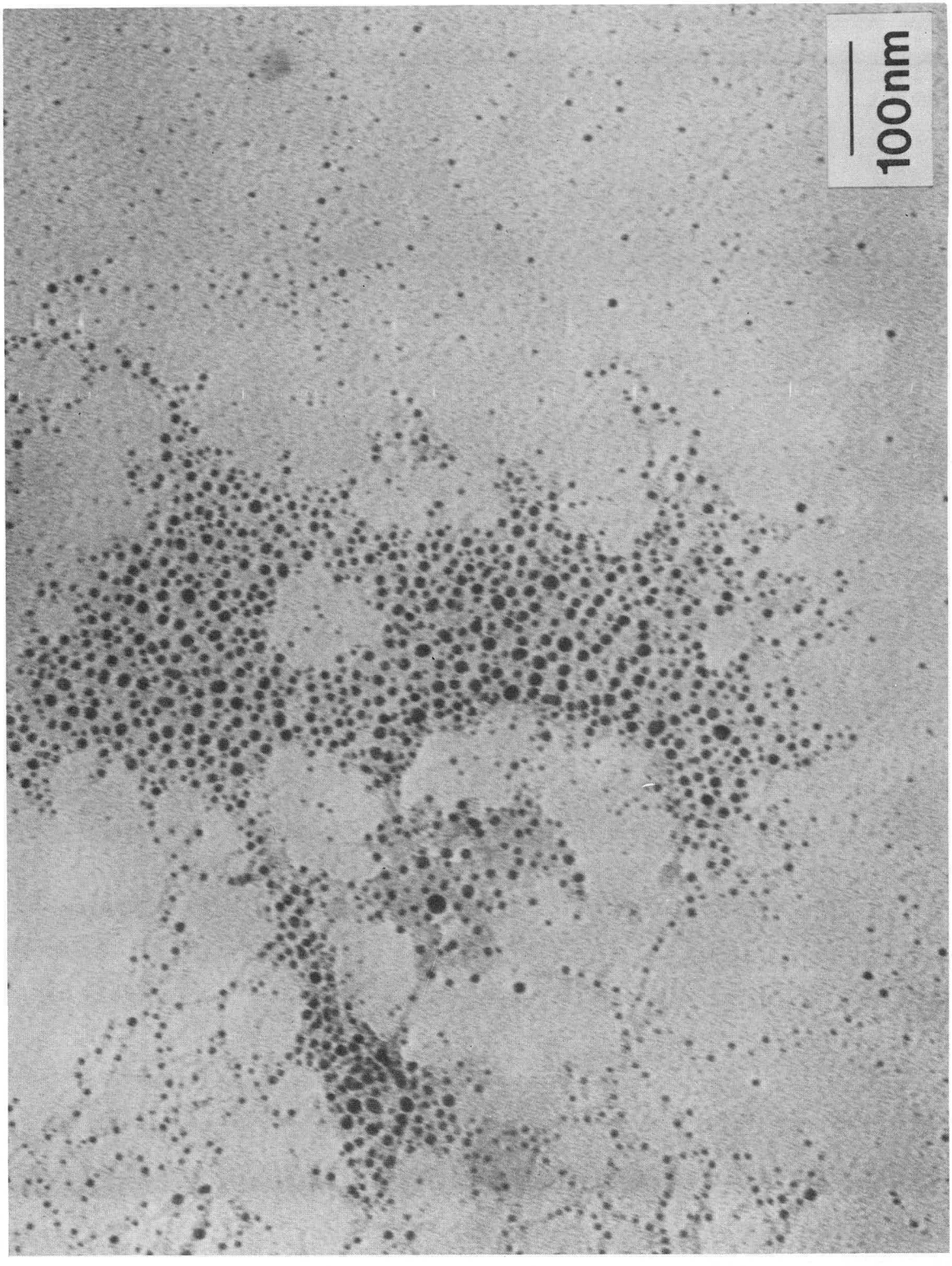

Fig. 15

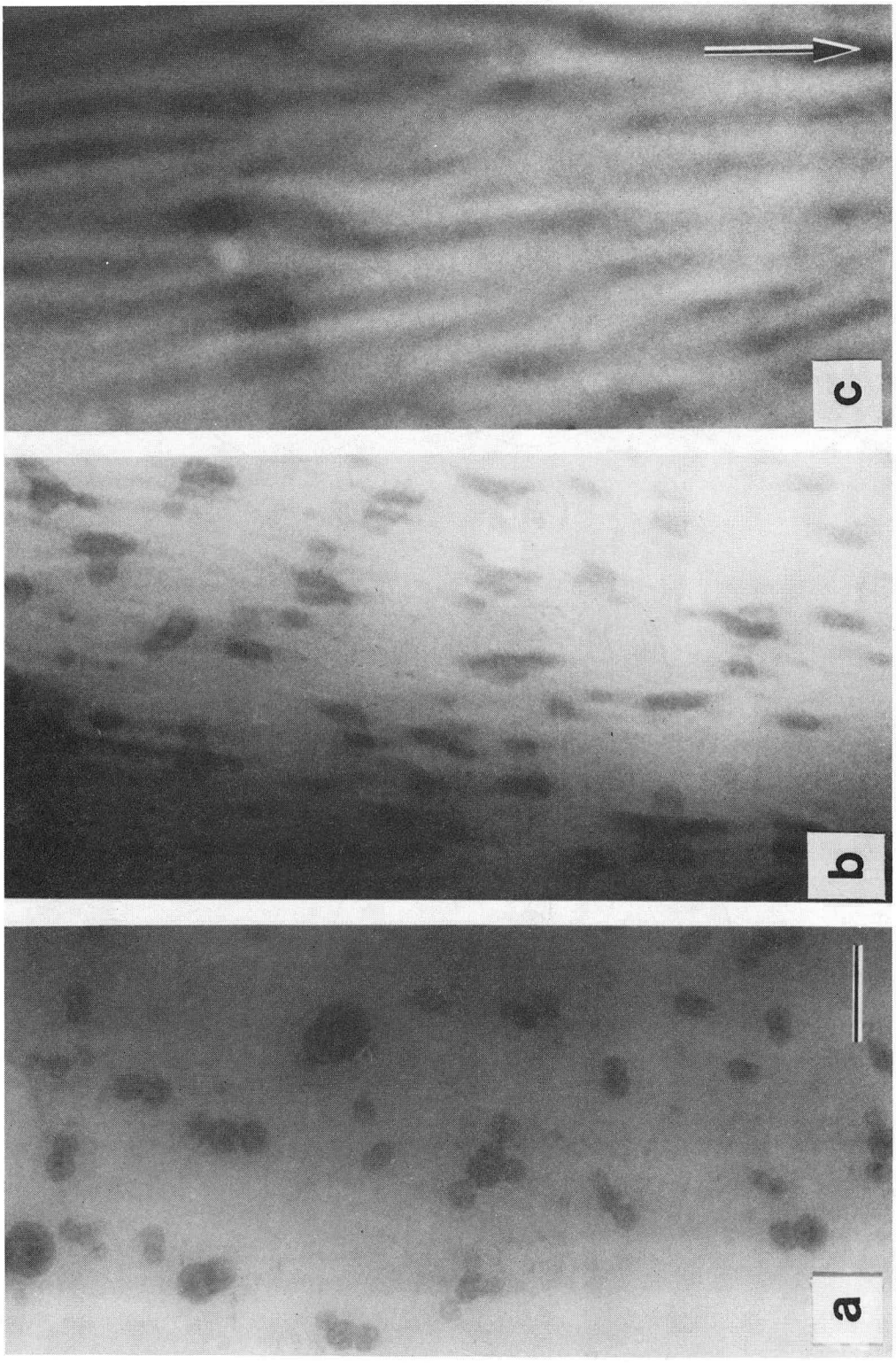

Fig. 16

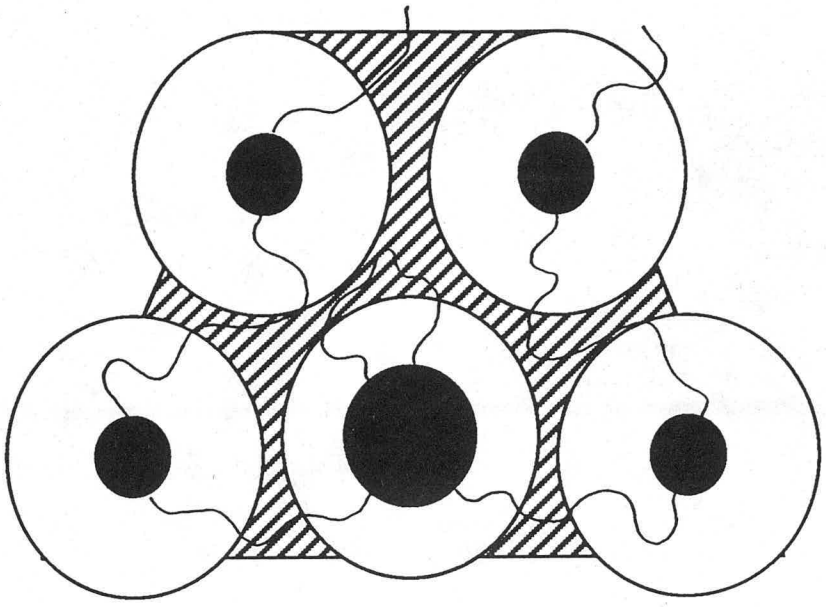

(a)

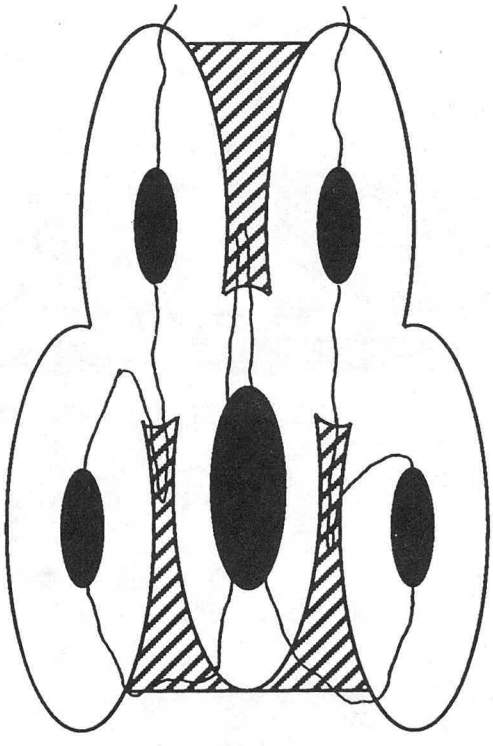

(b)

XBL 881-163

Fig. 17

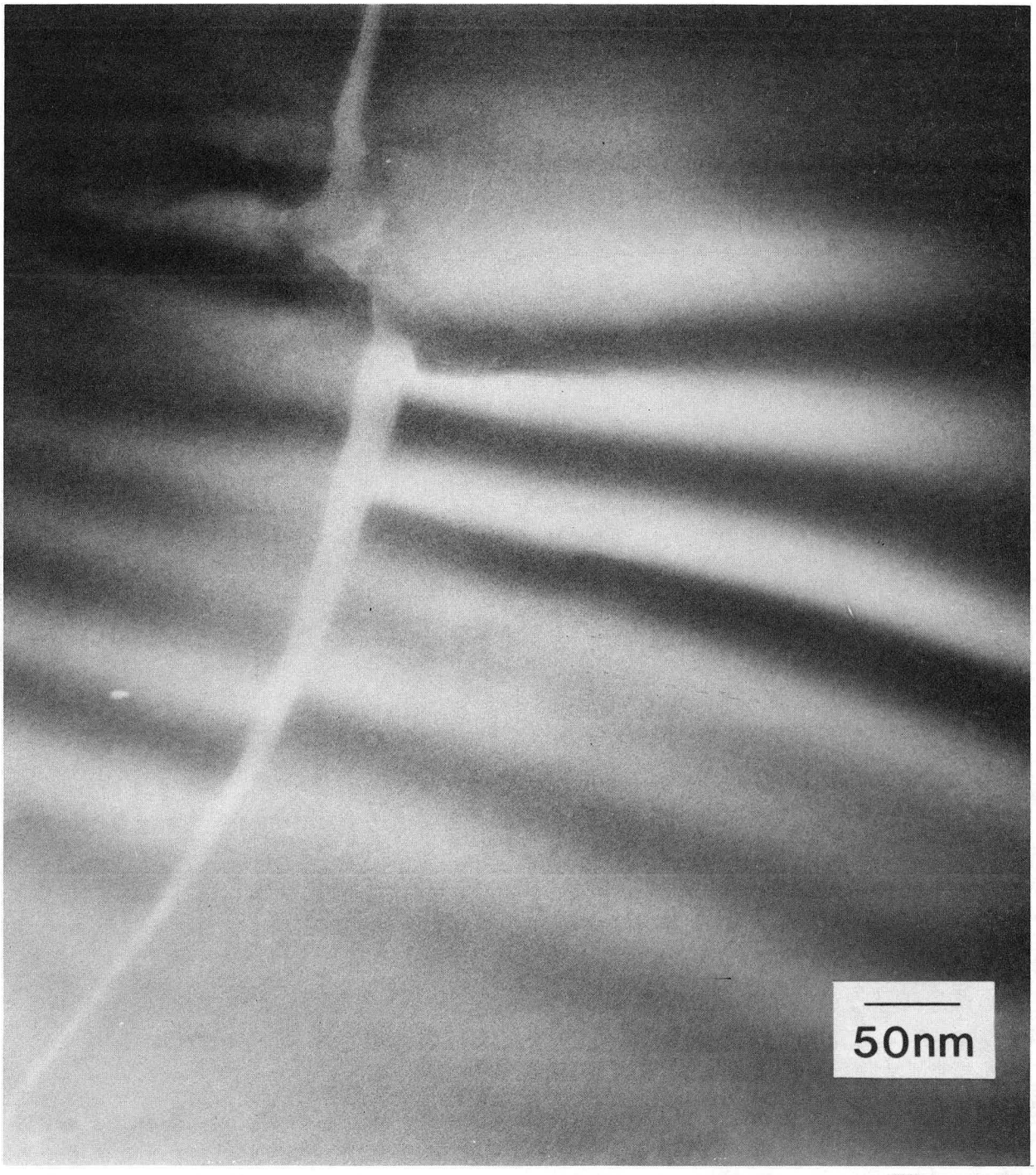

XBB 878-7105

Fig. 18

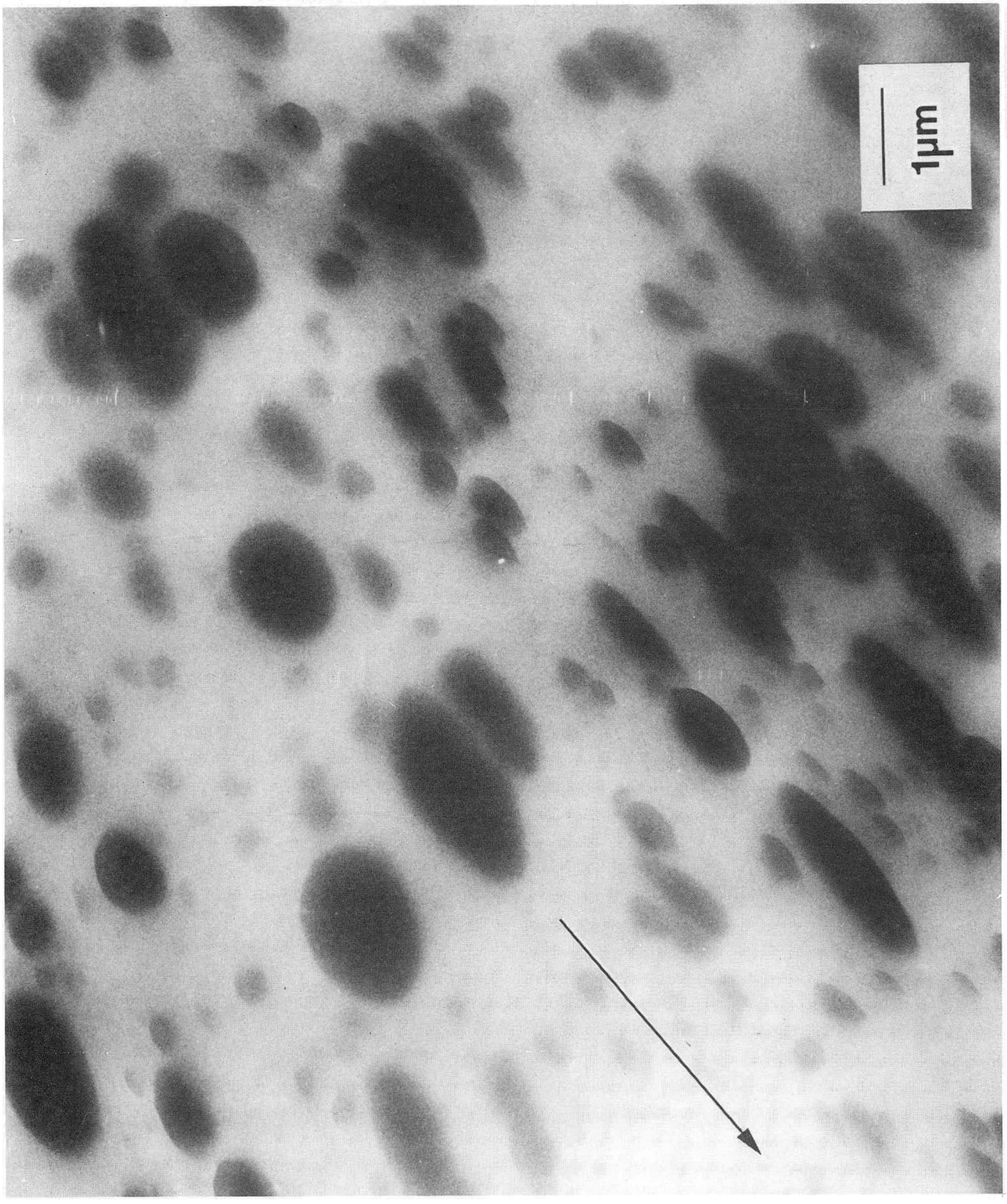

XBB 878-7099

Fig. 19

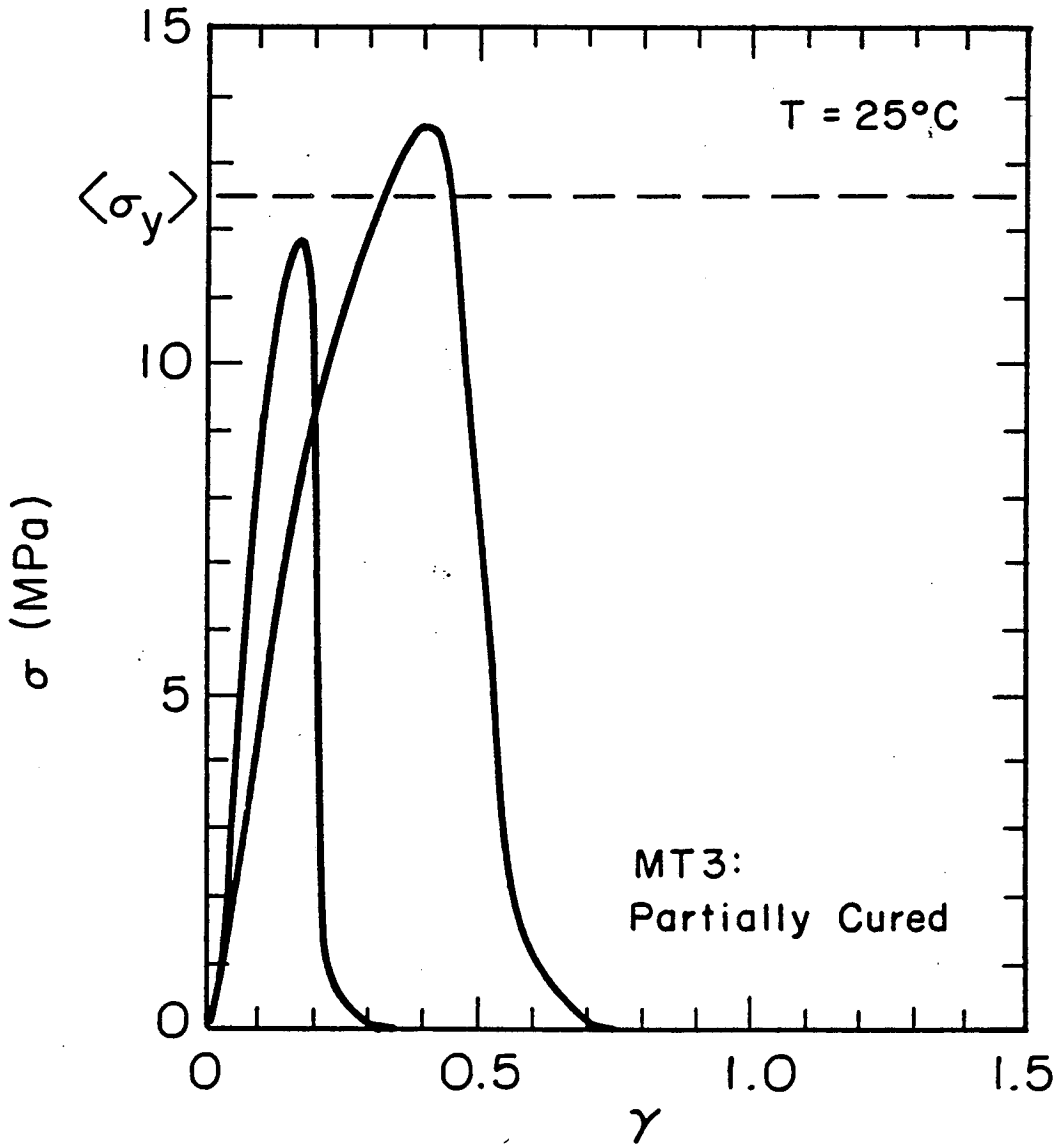

XBL 881-162

Fig. 20

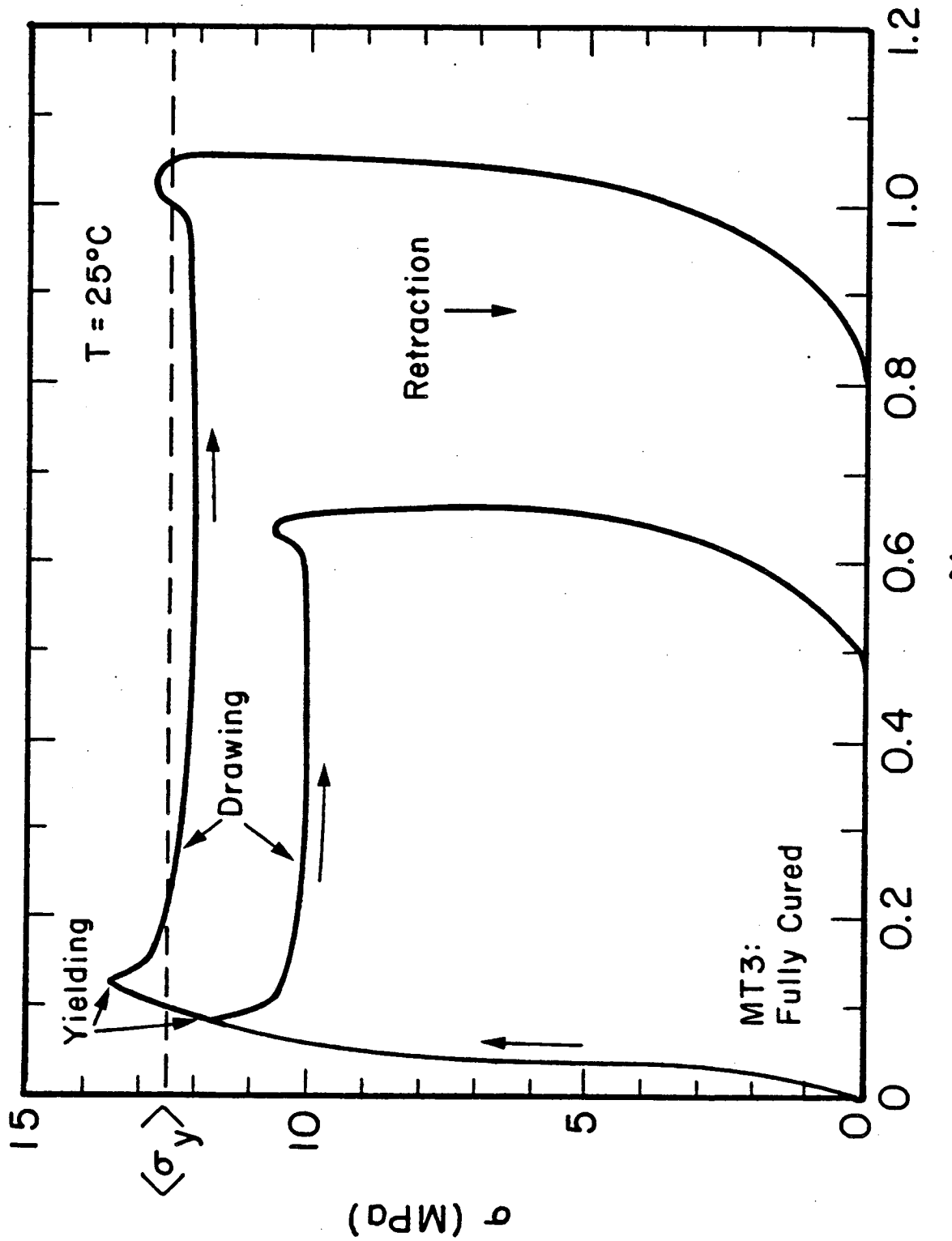

XBL 881-161

Fig. 21

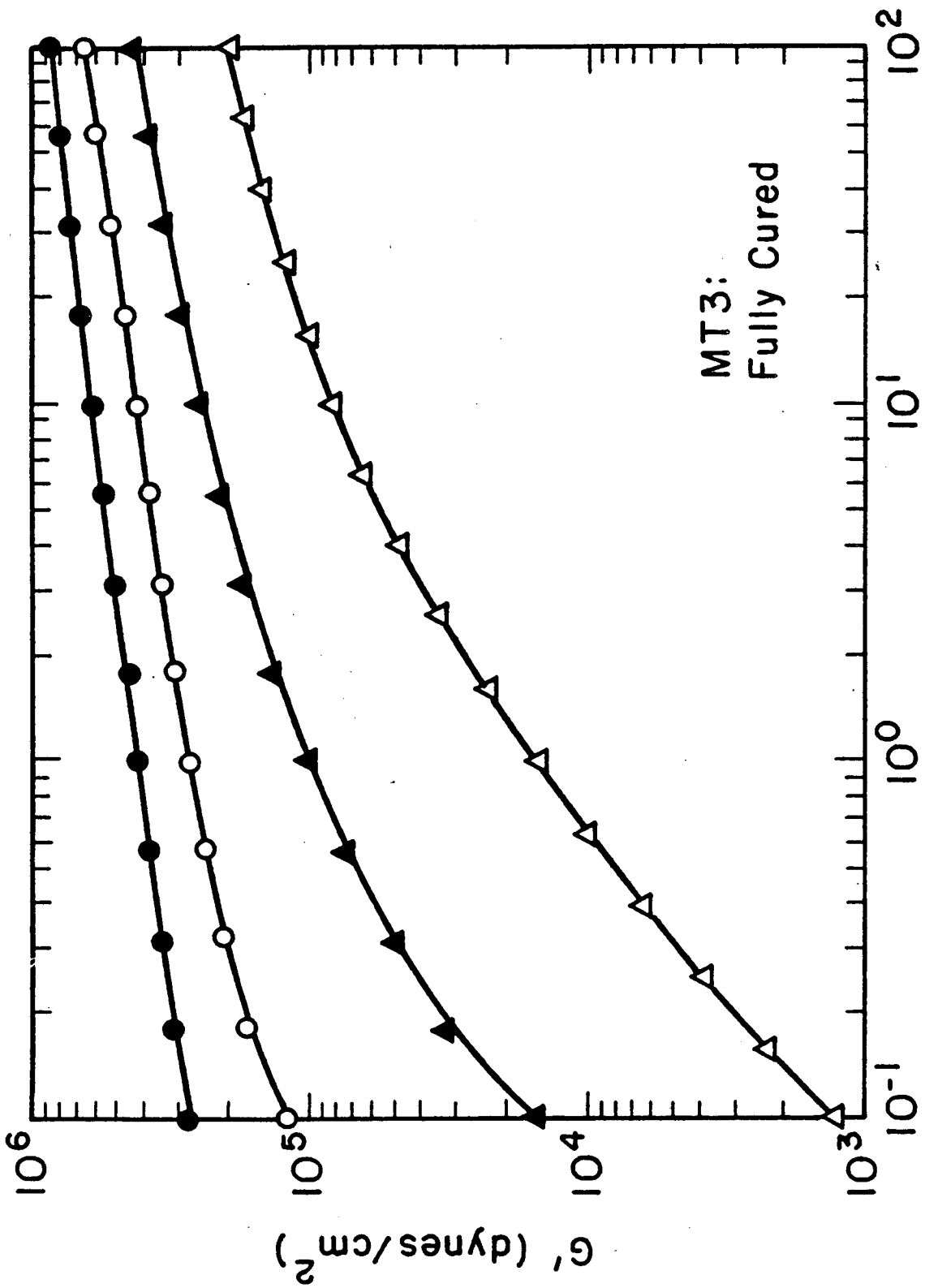

XBL 881-159

Fig. 22

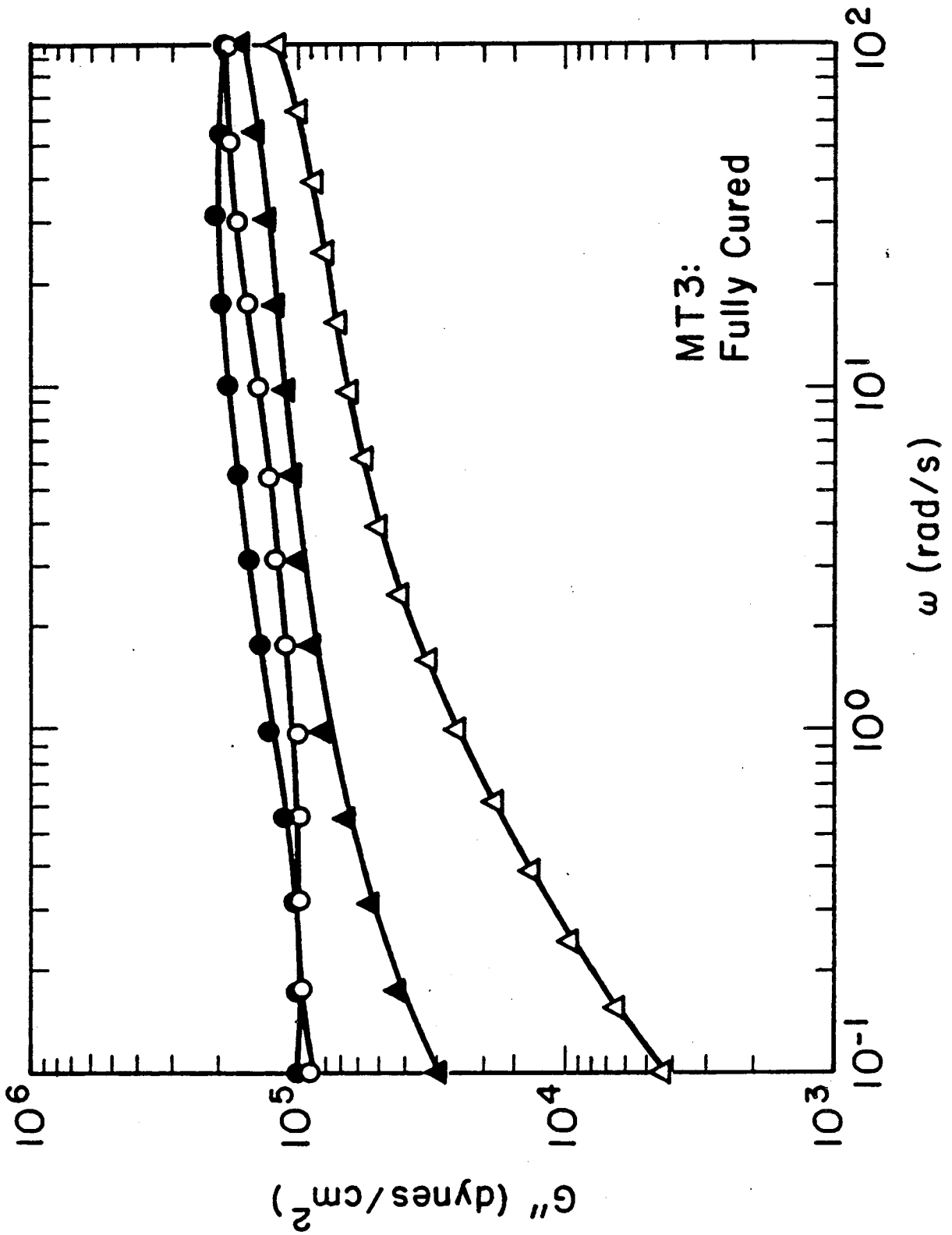

XBL 881-158

Fig. 23

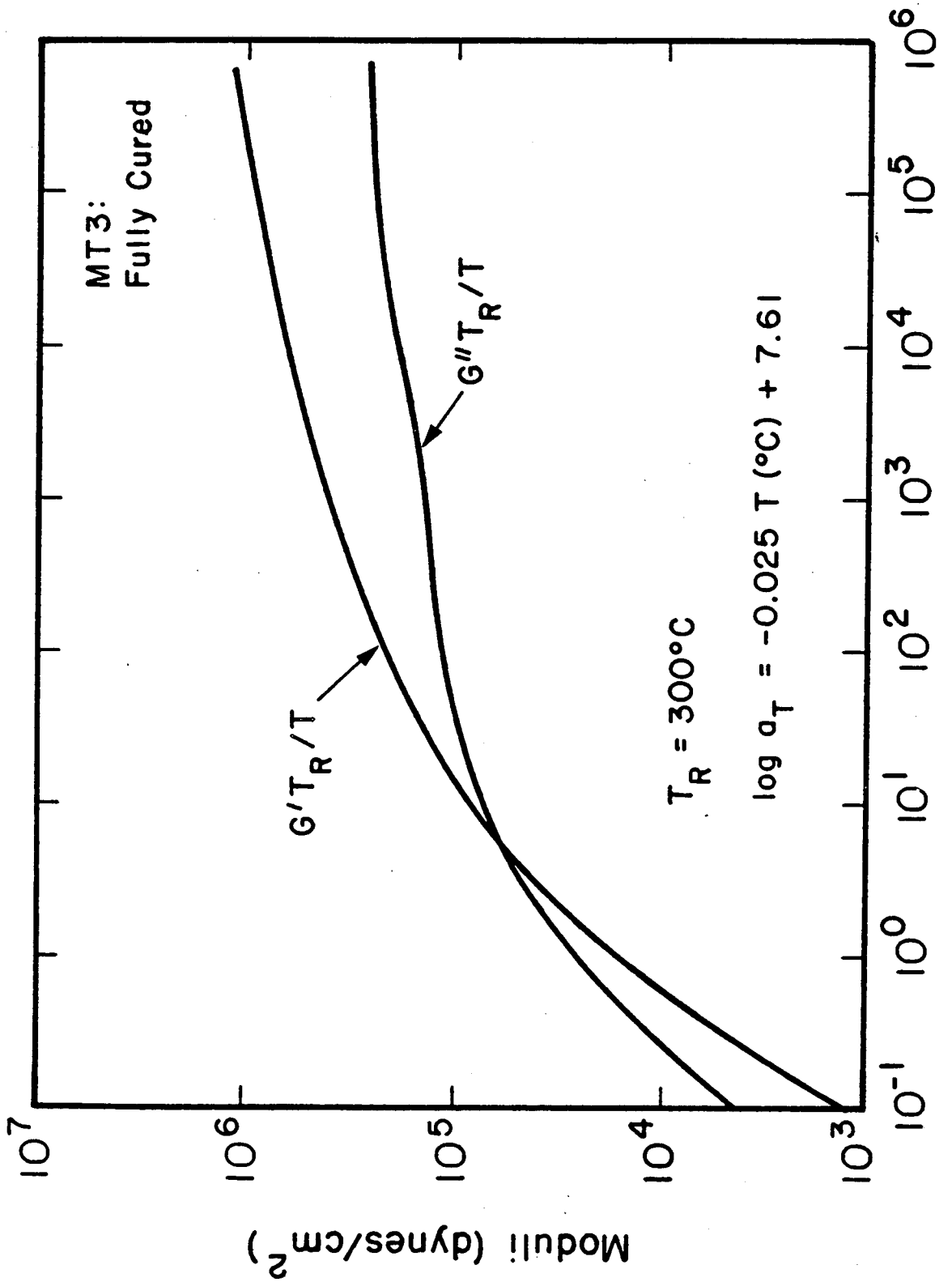

XBL 881-170

Fig. 24

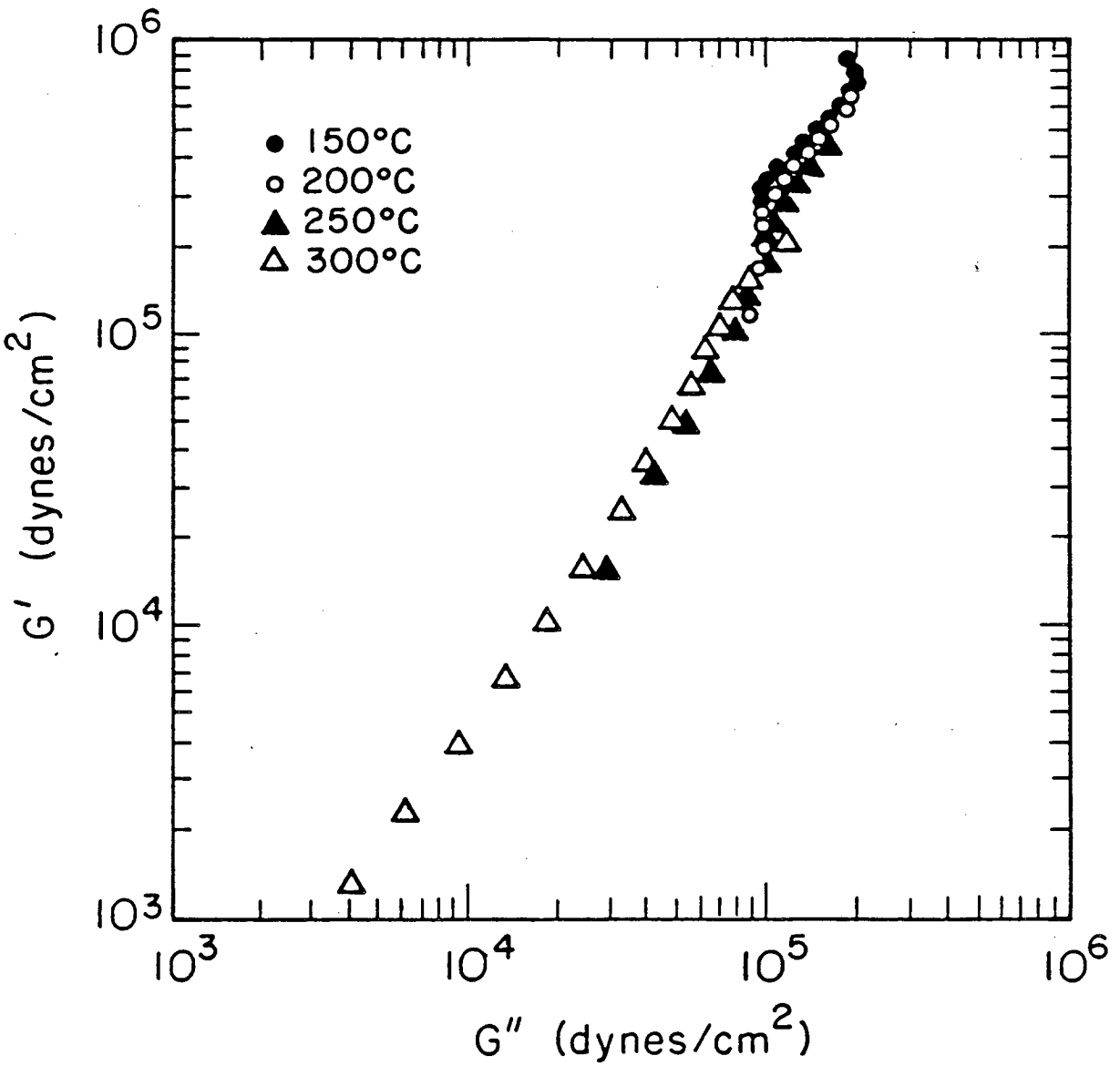

XBL 881-172

Fig. 25

LAWRENCE BERKELEY LABORATORY
TECHNICAL INFORMATION DEPARTMENT
UNIVERSITY OF CALIFORNIA
BERKELEY, CALIFORNIA 94720